1   **An autoregulation loop in *fust-1* for circular RNA regulation in *Caenorhabditis elegans***

2

3   Dong Cao

4

5   Information Processing Biology Unit, Okinawa Institute of Science and Technology Graduate
6   University, 1919-1 Tancha, Onna, Kunigami, Okinawa, Japan, 904-0495

7   Correspondence: dong.cao@oist.jp

8

9   **Abstract**

10

11   Circular RNAs (circRNAs) are always expressed tissue-specifically, suggestive of specific factors
12   that regulate their biogenesis. Here, taking advantage of available mutation strains of RNA binding
13   proteins (RBPs) in *Caenorhabditis elegans*, I performed a screening of circRNA regulation in
14   thirteen conserved RBPs. Among them, loss of FUST-1, the homolog of FUS (Fused in Sarcoma),
15   caused downregulation of multiple circRNAs. By rescue experiments, I confirmed FUST-1 as a
16   circRNA regulator. Further, I showed that FUST-1 regulates circRNA formation without affecting
17   the levels of the cognate linear mRNAs. When recognizing circRNA pre-mRNAs, FUST-1 can
18   affect both exon-skipping and circRNA in the same genes. Moreover, I identified an autoregulation
19   loop in *fust-1*, where FUST-1, isoform a promotes the skipping of exon 5 of its own pre-mRNA,
20   which produces FUST-1, isoform b with different N-terminal sequences. FUST-1, isoform a is the
21   functional isoform in circRNA regulation. Although FUST-1, isoform b has the same functional
22   domains as isoform a, it cannot regulate either exon-skipping or circRNA formation.

23

24

25   **Keywords**

26   circular RNA, FUS, RNA-binding protein, autoregulation, back splicing, alternative splicing

27

Introduction

29 Although treated as byproducts of splicing in early years (Cocquerelle et al., 1993; Nigro et al.,
30 1991), circRNAs have shown diverse functions in different biological or physiological
31 environments, including interactions with DNAs (transcription regulation (Li et al., 2015), R-loop
32 structure formation (Conn et al., 2017)), RNAs (miRNA sponge (Hansen et al., 2013; Memczak
33 et al., 2013)), and proteins (Du et al., 2020; Okholm et al., 2020; Xia et al., 2018; Zhu et al., 2019).
34 Rather than splicing errors, the circRNA production process is well-regulated, in which both
35 intronic sequences (*cis* elements) and RBPs (*cis/trans* elements) are involved (Chen, 2020).
36 Reverse complementary matches (RCMs, *cis* elements) in introns that flank exon(s) to be
37 circularized promote circRNA formation, presumably by bringing splice sites for back-splicing
38 together. RBPs (*cis/trans* elements) can regulate back-splicing positively or negatively.
39 Muscleblind in *Drosophila* promotes the production of the circRNA from the second exon of its
40 own pre-mRNA by binding to the flanking introns (Ashwal-Fluss et al., 2014). The splicing factor
41 Quaking promotes circRNA biogenesis during epithelial to mesenchymal transition (Conn et al.,
42 2015). Immune factors NF90/NF110 promote circRNA formation by associating with intronic
43 RNA pairs in circRNA-flanking introns (Li et al., 2017). RBM20 in mice promotes the production
44 of multiple circRNAs from the gene Tintin (Khan et al., 2016). ADAR1 (Ivanov et al., 2015;
45 Rybak-Wolf et al., 2015) and DHX9 (Aktas et al., 2017) negatively regulate circRNAs by
46 disturbing the base pairing of RCMs. Multiple heterogeneous nuclear ribonucleoproteins (hnRNPs)
47 and serine–arginine (SR) proteins function in a combinatorial manner to regulate circRNAs in
48 cultured *Drosophila* cells (Kramer et al., 2015). HNRNPL regulates circRNA levels in LNCaP
49 cells by binding to circRNA-flanking introns (Fei et al., 2017). A recent paper shows that RBP
50 FUS affects circRNA expression in stem cell-derived motor neurons in mice (Errichelli et al.,
51 2017). All these findings were from *in vitro* cultured cells of different organisms. *C. elegans*
52 provides a suitable animal model for *in vivo* study of circRNA regulation, given the conservation
53 of RBPs and availability of diverse mutant strains.

54 FUS plays diverse roles in DNA repair and RNA splicing (Sama et al., 2014). Particularly, the
55 mutation of FUS has been linked to the neurodegenerative disease ALS (Kwiatkowski et al., 2009;
56 Vance et al., 2009). *C. elegans* has been used to model ALS by knocking in wild-type or mutated
57 human FUS (Markert et al., 2019; Murakami et al., 2015; Murakami et al., 2012; Vaccaro et al.,
58 2012a; Vaccaro et al., 2012b; Veriepe et al., 2015). As the homolog of FUS in *C. elegans*, FUST-
59 1 is involved in lifespan and neuronal integrity regulation (Therrien et al., 2016) and miRNA-
60 mediated gene silencing (Zhang et al., 2018).

61 Autoregulation feedback has been found in many RBPs, which is beneficial for them to maintain
62 proper protein levels (Buratti and Baralle, 2011; Muller-McNicoll et al., 2019). The mechanisms
63 include autoregulation of alternative splicing (AS) of their own pre-mRNA, which either produces
64 unproductive transcripts with premature termination codons (PTCs) that are subjected to nonsense-
65 mediated decay (NMD) pathway (McGlincy et al., 2010; Rossbach et al., 2009; Sureau et al., 2001;
66 Wollerton et al., 2004) or produces another protein isoform with disturbed functional domains
67 (Damianov and Black, 2010). Here, I identified an autoregulation pathway in the production of the
68 two isoforms of FUST-1 in *C. elegans*.

69   Here, using available RBP mutation strains in *C. elegans*, I performed a screening of 13 conserved
70   RBPs in their roles in circRNA regulation. FUST-1 stood out in the screening, showing
71   promotional effects on the production of multiple circRNAs. I further checked FUST-1's role in
72   circRNA regulation globally by RNA-seq and found FUST-1 can also negatively regulate
73   circRNAs. FUST-1 recognizes pre-mRNAs of circRNA genes and can regulate both exon-
74   skipping and circRNA production in the same genes. Moreover, I characterized an autoregulation
75   loop in the production of the two isoforms of FUST-1, in which FUST-1, isoform a promotes the
76   skipping of exon 5 of *fust-1* pre-mRNA, which produces FUST-1, isoform b. Interestingly,
77   although FUST-1, isoform b has the same functional domains as isoform a, it cannot regulate exon-
78   skipping or circRNA formation.

79 **Results**

80 **1. RBP screening identifies FUST-1 as a circRNA regulator**

81 Previous studies have shown that circRNAs are expressed in a tissue-specific and well-regulated
82 manner (Chen and Schuman, 2016; Gruner et al., 2016; Memczak et al., 2013; Rybak-Wolf et al.,
83 2015; Westholm et al., 2014; You et al., 2015), suggesting the existence of specific factors that
84 regulate circRNA production. Here, taking advantage of the available RBP mutants in *C. elegans*,
85 I aimed to identify potential circRNA regulators. Several previously identified circRNAs that were
86 either neuron-enriched or highly expressed in neurons were selected as targets (Figure S1A) (Cao,
87 2021). Thirteen RBPs that are conserved and have expressions in the neurons were chosen as
88 potential regulators (Norris et al., 2017). Using mutant strains of these RBPs, a screening by RT-
89 qPCR was performed to check the level changes of selected circRNAs in these mutant strains
90 compared with wild-type N2 strain at the L1 stage (Figure 1A). As expected, levels of some
91 circRNAs were altered in these mutant strains. Interestingly, most level changes of the selected
92 circRNAs in these mutants were downregulations, suggestive of these RBPs' beneficial roles in
93 circRNA production. Moreover, multiple neuron-enriched circRNAs (*circ-glr-2*, *circ-iglr-3*, *circ-
94 arl-13*, *circ-cam-1*) were found to be downregulated in several strains (*asd-1(csb32)*, *tiar-3(csb35)*,
95 *fox-1(csb39)*, *mec-8(csb22)*, *hrpf-1(csb26)*, and *fust-1(csb21)*), suggesting the regulation of these
96 circRNAs by multiple RBPs. This is consistent with their roles in alternative splicing, where
97 combinational regulation of one target by multiple RBPs is common in *C. elegans* (Tan and Fraser,
98 2017). No additive effect in circRNA regulation was found in *fust-1(csb21); hrpf-1(csb26)* double
99 mutant strain compared with *fust-1(csb21)* single mutation (Figure S1B), suggesting that these
100 RBPs may function as parts of a whole RNA-protein complex.

101 In these strains, *fust-1(csb21)* showed the most substantial downregulation of multiple circRNAs
102 (Figure 1A). Hence it was chosen for further investigation. The downregulation of these circRNAs
103 was also found in another *fust-1* mutant strain *fust-1*(*tm4439)* (Figure 1B and Figure S1C). To
104 further confirm the role of *fust-1* in circRNA regulation, a rescue strain (*fust-1(csb21); Ex[fust-
105 1::mRFP]*) and an overexpression strain (N2; *Ex[fust-1::mRFP]*) were made with
106 extrachromosomal expression of *fust-1* genomic sequence, starting from *fust-1* promoter (2181 bp
107 upstream ATG) to just before the stop codon of *fust-1*. Monomeric red fluorescent protein (mRFP)
108 was fused to the C-terminal to check expression patterns. The expression of FUST-1 was mainly
109 in the nucleus of neurons and intestinal cells (Figure 1C and S1D). The mRFP-positive L1 worms
110 from the rescue strain and the overexpression strain were sorted, and levels of the circRNAs were
111 checked by RT-qPCR. As expected, the levels of downregulated circRNAs were restored in the
112 rescue strain, confirming *fust-1*'s role in promoting circRNA production (Figure 1D). The *fust-
113 1(csb21)* strain also showed another phenotype of lower average moving speed at day three adult
114 stage when cultured at 25ºC, which was also recovered in the rescue strain (Figure S1E). Although
115 multiple copies of *fust-1* existed in the extrachromosomal arrays of the rescue and the
116 overexpression strain (Figure S1F), these strains did not show much further improvement in
117 circRNA levels or improvement in locomotion speed (Figure 1D and Figure S1E). This may be
118 because of post-transcriptional regulation of *fust-1* or saturation of FUST-1 protein.
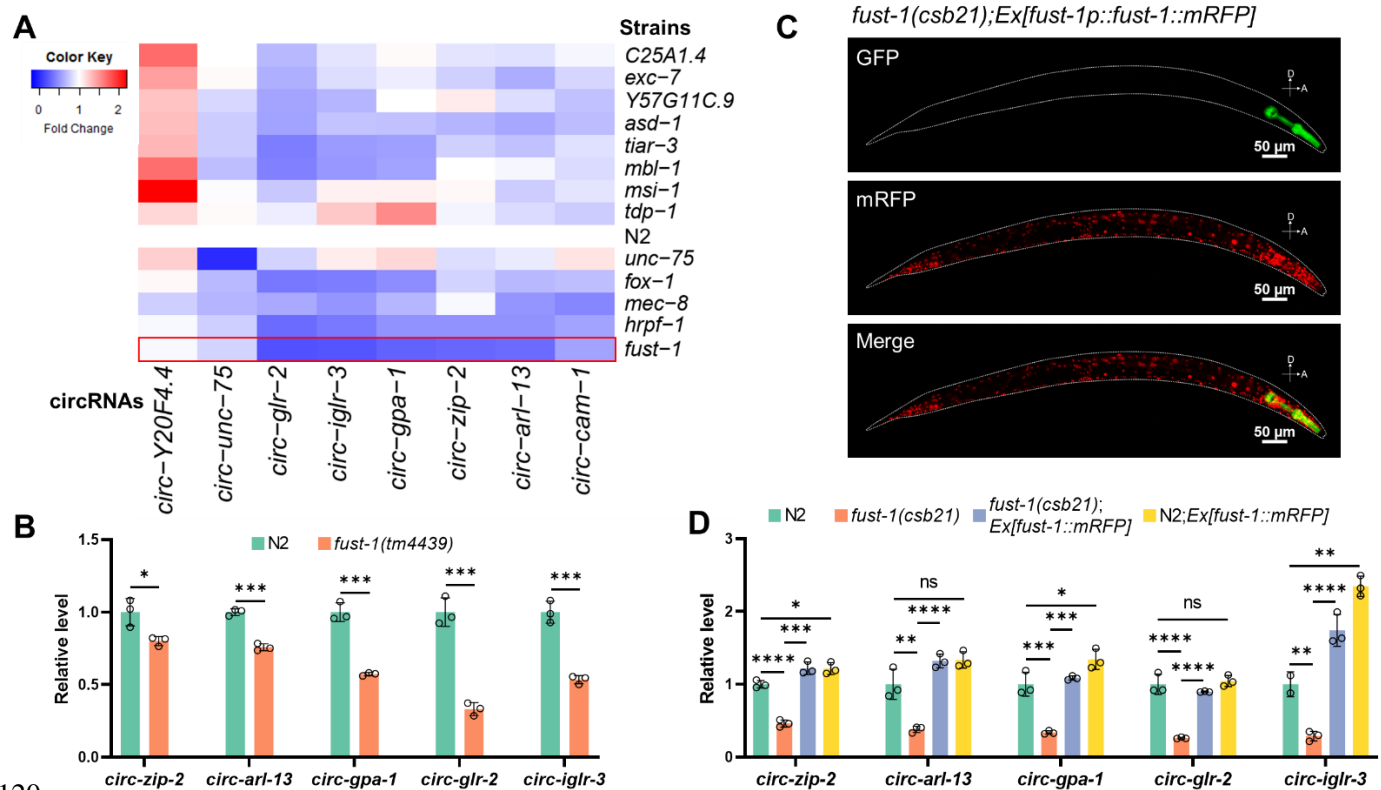
119

Figure 1. RBP screening identifies FUST-1 as a circRNA regulator

(A) Heatplot showing the fold changes of circRNAs in 13 RBP mutant strains compared with wild-type N2 strain. Foldchanges are quantified by RT-qPCR and normalized to the N2 strain using *pmp-3* as the reference gene. Blue color means downregulation and red color means upregulation.

(B) RT-qPCR quantification of circRNA levels in wild-type N2 strain and *fust-1(tm4439)* strain. Levels are normalized to the N2 strain using *pmp-3* as the reference gene. Results are shown as mean ± sd of three biological replicates. Two-tailed Student's *t*-test. $p<0.05$, **$p < 0.01$, ***$p < 0.001$.

(C) Representative images showing the expression pattern of mRFP-fused FUST-1 in *fust-1(csb21)* strain. Note the pharyngeal GFP expression in *fust-1(csb21)*. Scale bars: 50 μm.

(D) RT-qPCR quantification of circRNAs in the indicated strains. Levels are normalized to the N2 strain using *pmp-3* as the reference gene. Results are shown as mean ± sd of three biological replicates. One-way ANOVA, Tukey's multiple comparisons. *$p<0.05$, **$p < 0.01$, ***$p < 0.001$, ****$p < 0.0001$; ns, not significant.

2. FUST-1 regulates circRNAs without affecting the cognate linear mRNAs

Next, to clarify whether FUST-1 promotes circRNA production by transcription promotion or not, levels of circRNAs and their cognate linear mRNAs were compared between the N2 strain and *fust-1(csb21)* strain at the L1 stage. While levels of these circRNAs were downregulated, their linear mRNA levels were not affected by the loss of FUST-1 (Figure 2A), indicating that FUST-1's role in circRNA production is not through promoting transcription. Northern blot detection of the linear and circular transcript of *zip-2* also showed the same trend, in which circRNA was downregulated, whereas linear mRNA was not affected (Figure 2B and Figure 2C).

To check the regulation of circRNA by FUST-1 globally, I performed RNA sequencing (RNA-seq) with ribosomal RNA depletion to compare differentially expressed circRNAs between *fust-1(csb21)* strain and wild-type N2 strain at the L1 stage. circRNA annotation was performed using DCC (Cheng et al., 2016), and differential expression was performed using DESeq2 (Love et al., 2014). Both mRNAs and circRNA clustered separately in principal component analysis (PCA) plots (Figure S2A and S2B). In total, 1266 circRNAs from 1199 annotated genes and 20 not-annotated loci were obtained with at least three back-splice junction (BSJ) reads in either group, with 916 in N2 strain and 849 in *fust-1(csb21)* strain (Figure 2D and Table S5). TPM (transcripts per million reads) values of circRNAs were compared between the two strains. circRNAs in the N2 strain showed significantly higher TPM values than those in *fust-1(csb21)* strain (paired Wilcoxon test, $p < 2.2e\text{-}16$) (Figure 2E), indicating general promotional roles of FUST-1 in circRNA production, although some circRNAs were also upregulated without FUST-1 (Table S6). Then, to check whether level changes in circRNA correlate with their cognate linear mRNAs, the fold changes of circRNA were plotted against those of their cognate mRNAs (Table S7), which showed a weak correlation (Pearson's correlation coefficient $R = 0.27$, $p = 3.5e\text{-}05$) of circRNAs with baseMean (given by DESeq2) bigger than 3 (Figure 2F). The correlation was even weaker when all the circRNAs from annotated genes were considered (Figure S2C, Pearson's correlation coefficient $R = 0.14$, $p = 7.4e\text{-}07$). These results were consistent with the finding that FUST-1 regulates circRNAs without disturbing the cognate linear mRNA levels (Figure 2A).

In my previous study, I provided the first neuronal circRNA profiles at the L1 stage of *C. elegans* (Cao, 2021). I then asked whether FUST-1 has a preference in the regulation of neuronal circRNAs. The circRNAs identified in this work (the "N2-*fust-1(csb21)*" dataset) were compared with my previous dataset (the "sort & whole" dataset), which resulted in 726 overlapped circRNAs (Figure S2D). Fold changes of the 726 overlapped circRNAs between N2 and *fust-1(csb21)* were plotted against those between the sort group (sorted neuron samples) and the whole group (whole worm samples), which showed no correlation (Figure 2G, Pearson's correlation coefficient $R = -0.038$, $p = 0.3$), suggesting that FUST-1 has no preference for neuronal circRNAs.
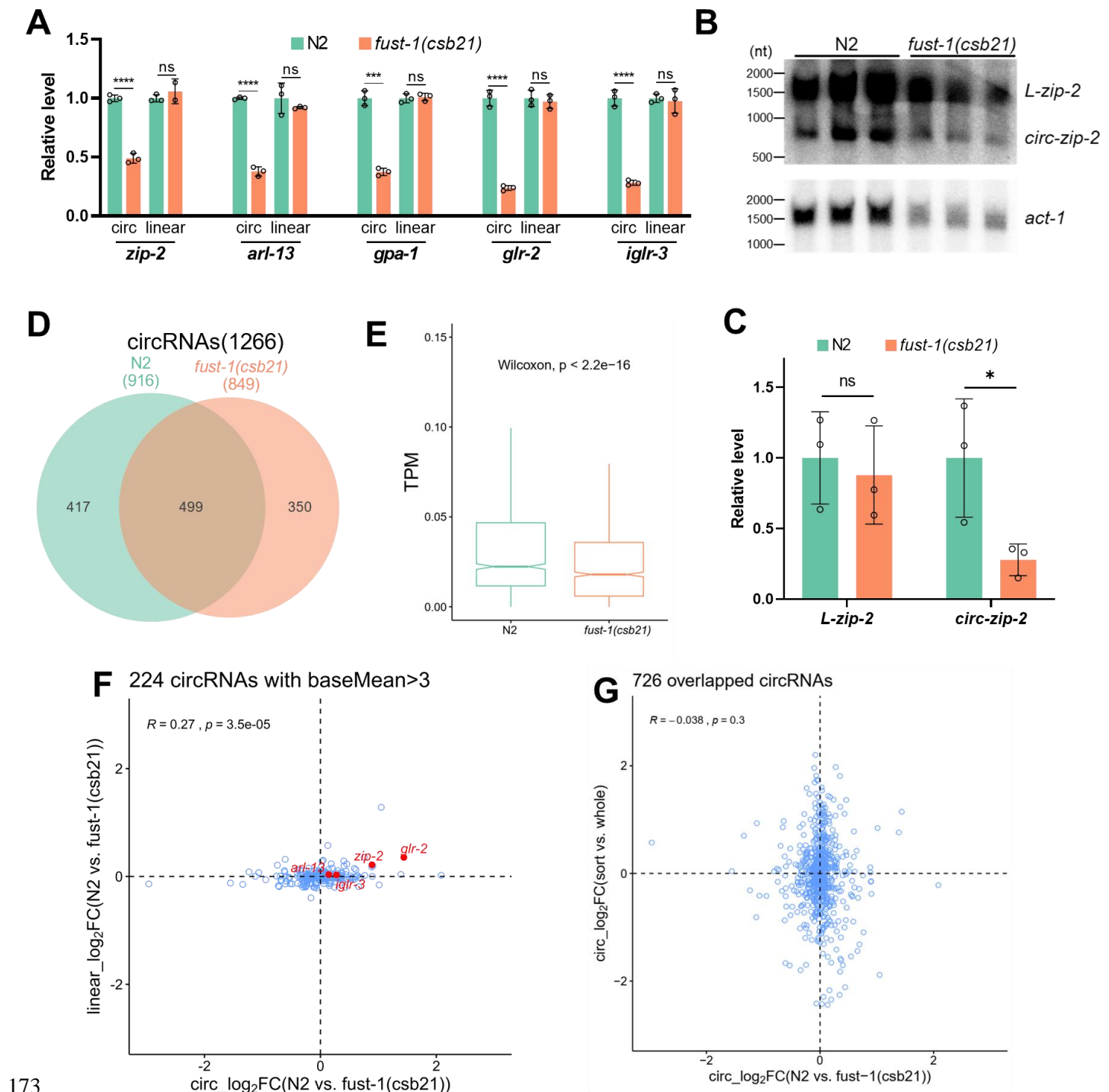
Figure 2. FUST-1 regulates circRNAs without affecting the cognate linear mRNAs

(A) RT-qPCR quantification of circRNAs and their linear mRNAs in the N2 strain and *fust-1(csb21)* strain. Levels are normalized to the N2 strain using *pmp-3* as the reference gene. Results are shown as mean ± sd of three biological replicates. Two-tailed Student's *t*-test. ***$p < 0.001$, ****$p < 0.0001$; ns, not significant.

179   (B) Northern blot detection *zip-2* transcripts, both linear and circular, and *act-1* in the L1 stage of
180   N2 strain and *fust-1(csb21)* strain.

181   (C) Quantification of northern blot results in (B), normalized to N2 strain using *act-1* as the
182   reference gene. Results are shown as mean ± sd. Two-tailed Student's *t*-test. *$p < 0.05$; ns, not
183   significant.

184   (D) Overlap of circRNAs detected in the RNA-seq results of N2 strain and *fust-1(csb21)* strain.

185   (E) TPM (transcripts per million reads) comparison of all circRNAs between N2 and *fust-1(csb21)*.
186   *P* value indicates paired Wilcoxon test.

187   (F) Scatter plot showing the log2 fold changes of 224 circRNAs with baseMean > 3 versus log2
188   fold changes of their corresponding linear mRNAs. The Pearson correlation coefficient (*R*) and *p*
189   value (*p*) are shown. Names of several circRNA genes are labeled.

190   (G) Scatter plot showing the log2 fold changes of 726 overlapped circRNAs between the "N2-*fust-*
191   *1(csb21)*" dataset and the "sort-whole" dataset. The Pearson correlation coefficient (*R*) and *p* value
192   (*p*) are shown.

193

3. FUST-1 binds to pre-mRNAs of circRNA genes

FUS binds to flanking introns of circRNA genes in N2a cells (Errichelli et al., 2017). I next checked whether FUST-1 in *C. elegans* recognizes pre-mRNAs of circRNA genes to regulate circRNA formation. Using CRISPR-Cas9 technology, I inserted the FLAG tag to the N terminal, just after the start codon, or to the C-terminal, just before the stop codon, respectively (Figure 3A and Figure S3A). The effect of FLAG-tag insertion on FUST-1's role in circRNA regulation was evaluated. While N-terminal FLAG insertion showed slight increases in circRNA levels, C-terminal FLAG tag fusion affected FUST-1's function in circRNA regulation in multiple circRNAs (Figure S3B and S3C). Hence N-terminal FLAG fused FUST-1 strain was used for the co-immunoprecipitation (Co-IP) experiment. Dynabeads Protein G conjugated with anti-FLAG antibody (+Ab) were used for Co-IP. Beads only (-Ab) were used as the negative control. As expected, the anti-FLAG antibody successfully enriched FLAG::FUST-1 after Co-IP (Figure 3B and Figure S3D). Then the levels of pre-mRNAs of circRNA genes were quantified by RT-qPCR. Threshold cycle (Ct) values were used for comparison. Lower Ct values indicate higher levels. While rRNA control (*18S rRNA* and *26S rRNA*) was depleted after Co-IP, all the pre-mRNAs of circRNA genes were enriched compared with input samples (Figure 3C). Moreover, these pre-mRNAs showed significate lower Ct values than those of control groups without using of antibody (Figure 3C), suggesting that FUST-1 binds to pre-mRNAs of the circRNAs genes to regulate circRNA formation.
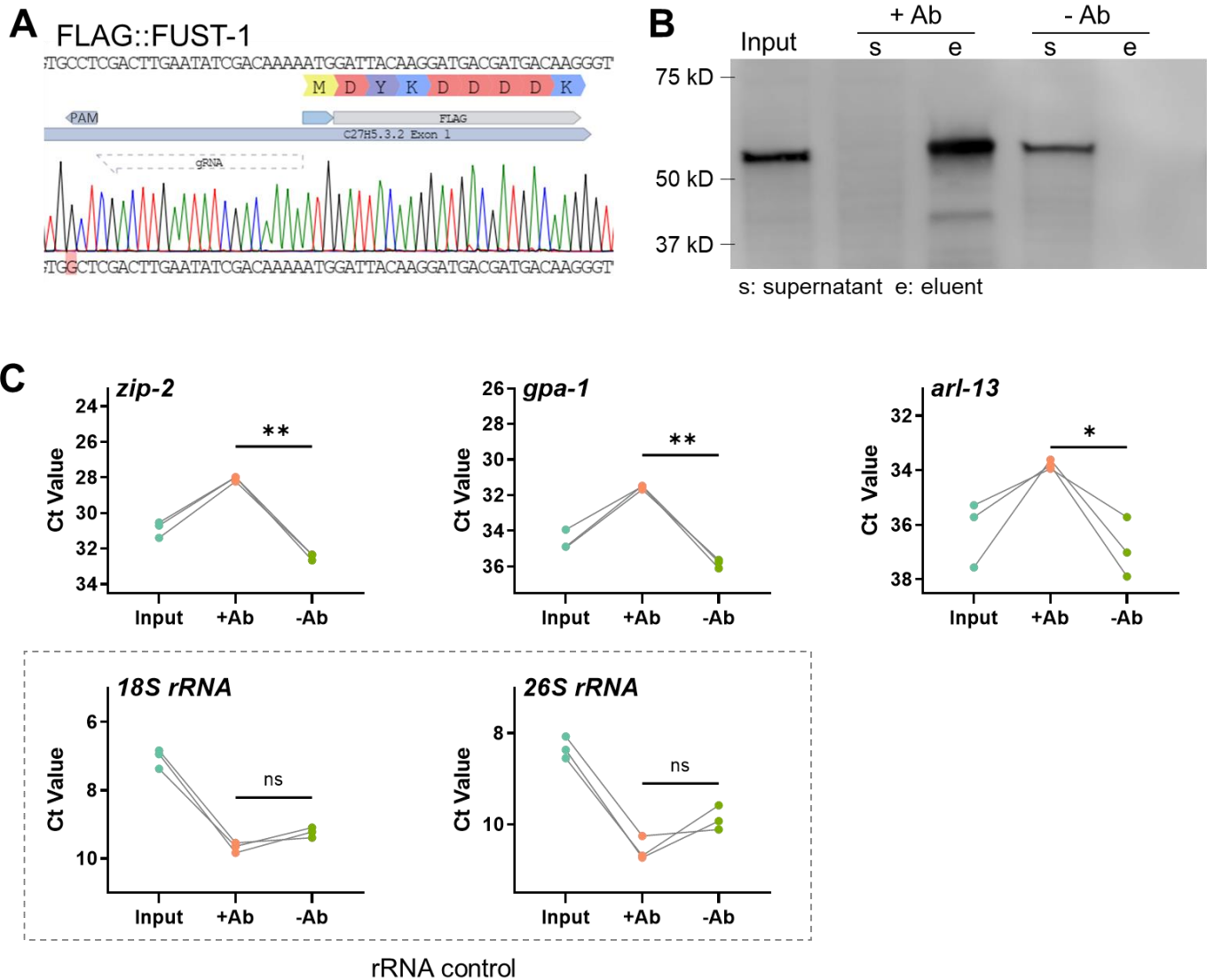
Figure 3. FUST-1 binds to pre-mRNAs of circRNA genes

(A) Sequence confirmation for N-terminal fusion of FLAG tag just after the start codon of FUST-1. Note the position of gRNA and the mutated PAM site (AGG>AGC).

(B) Western blot showing the co-immunoprecipitation (Co-IP) of FLAG::FUST-1.

(C) Ct value changes of pre-mRNAs of some circRNA genes before and after Co-IP of FLAG::FUST-1 with or without anti-FLAG antibody. Results from 3 biological replicates are shown. Paired two-tailed Student's t-test. *$p < 0.05$, **$p < 0.01$, ns, not significant.

224   **4. FUST-1 regulates both exon-skipping and back-splicing**

225   In my previous study, transcripts that skip the exons to be circularized were identified in several

226   circRNA genes (Cao, 2021). As the homolog of FUST-1 in humans and mice, FUS is involved in

227   the regulation of AS of many genes by binding to their pre-mRNAs (Dichmann and Harland, 2012;

228   Ishigaki et al., 2012; Rogelj et al., 2012). Since FUST-1 binds to the pre-mRNAs of these circRNA

229   genes, I then checked whether FUST-1 could also regulate exon-skipping or not. In *zip-2*, reads

230   aligned to the skipped junction were much less in *fust-1(csb21)* strain (27.0 reads on average) than

231   those in wild-type N2 strain (71.3 reads on average) (Figure 4A). The RT-qPCR quantification

232   results also showed that both the circRNA and the skipped transcript in *zip-2* were downregulated

233   without FUST-1 (Figure 4B). In *arl-13*, while the circRNA got downregulated in *fust-1(csb21)*,

234   the skipped transcript was weakly upregulated (Figure 4C). These results suggest that FUST-1

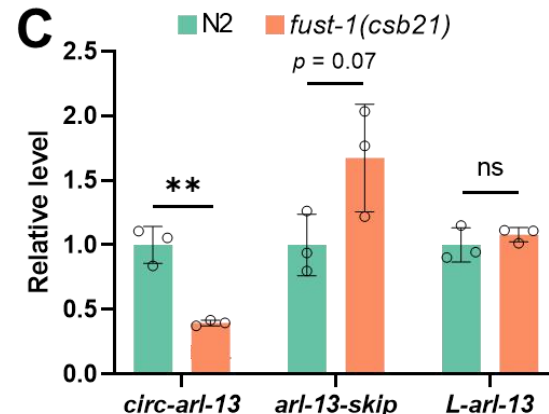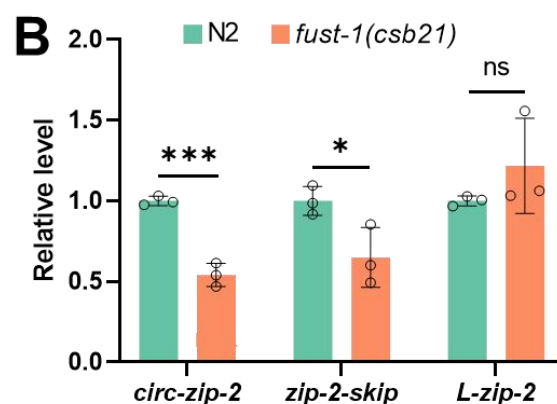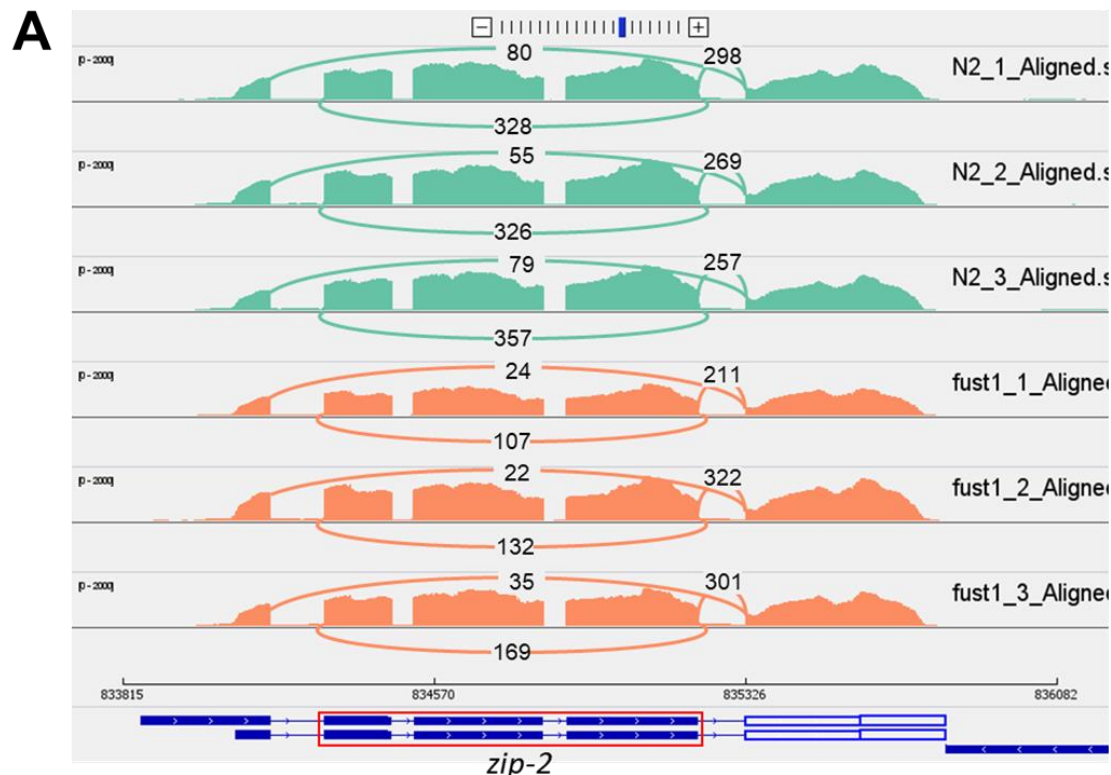235   may function differently in different genetic environments.

236

237

Figure 4. FUST-1 regulates both exon-skipping and back-splicing.

(A) Sashimi plot showing numbers of reads aligned to the canonical splice junction, the skipped junction, and the back-splice junction in *zip-2*. Exons in the red rectangle are circularized.

(B, C) RT-qPCR quantification of levels of the circular, skipped, and full-length linear transcripts in *zip-2* (B) and *arl-13* (C) between wild-type N2 strain and *fust-1(csb21)* strain. Levels are normalized to the N2 strain using *pmp-3* as the reference gene. Results are shown as mean ± sd of three biological replicates. Two-tailed Student's *t*-test. *$p < 0.05$, **$p < 0.01$, *** $p < 0.001$, ns, not significant.

247 ### 5. An autoregulation loop in *fust-1*

248 FUST-1 protein has two isoforms: isoform a is from the full-length transcript, and isoform b is
249 from the transcript with skipped exon 5 (Figure 5A). Moreover, isoform b is translated using a
250 downstream AUG and a different reading frame (+1) compared with isoform a. The reading frame
251 in isoform b becomes the same as in isoform a after the skipping of exon 5 (38 nt in length). This
252 results in a shorter isoform b with different N-terminal sequences, but the RNA recognition motif
253 (RRM), zinc-finger (ZnF) domain, and the nuclear localization signal (NLS) domain are the same
254 as isoform a (Figure 5A). To check how these two isoforms are expressed, two plasmids with
255 different colors and a nonsense mutation in the reading frame of either isoform a (*fust-1a-*
256 *mut::mRFP*) or isoform b (*fust-1b-mut::GFP*) were constructed so that only the other isoform can
257 be expressed (Figure 5A and Figure S4A). Co-injection of the two plasmids in wild-type N2 strain
258 showed that the two isoforms of FUST-1 were co-expressed in the nucleus of the same cells:
259 neurons and intestinal cells (Figure 5B and Figure S4B). Interestingly, in early eggs, isoform a was
260 expressed earlier than isoform b (Figure 5C). Furthermore, *fust1a-mut::GFP* plasmid expressed
261 faintly in *fust-1(csb21)* strain and co-injection with *fust1b-mut::mRFP* can increase the GFP
262 intensity (data not shown). These results gave a hint that isoform a may promote the production of
263 isoform b.

264 To prove this hypothesis, I constructed a dual-color splicing reporter (Norris et al., 2014;
265 Thompson et al., 2019) of the skipping of exon 5 in *fust-1* (Figure S4C), in which no skipping
266 gives GFP expression while skipping of exon 5 results in mCherry expression. As expected, two
267 colors were co-expressed in almost all the neurons in wild-type strain (Figure 5D), suggesting that
268 exon-skipping of exon 5 is happening in all the neurons. However, when the reporter plasmid was
269 crossed into two *fust-1* mutation strains, *fust-1(csb21)* and *fust-1(tm4439)* (Figure S1C), the
270 expression of mCherry was dramatically reduced (Figure 5D and Figure S4D), indicating FUST-
271 1 was involved in the exon-skipping of its own pre-mRNA. Since *fust-1(csb21)* strain has
272 pharyngeal GFP expression (Norris et al., 2017) (Figure S1C and Figure 5D), neurons in the ventral
273 nerve cord around the neck were used to quantify the mCherry-to-GFP intensity ratios (Figure 5D).
274 The mCherry-to-GFP ratios were significantly reduced in both two *fust-1* mutants, and they did
275 not change in the *mec-8(csb22)* strain (Figure 5E and Figure S4D).

276 Next, to prove that FUST-1, isoform a promotes the skipping of exon 5 of *fust-1* pre-mRNA, I
277 tried the rescue of mCherry expression of the splicing reporter in *fust-1(csb21)* by co-injection of
278 the reporter plasmid with FUST-1, isoform a cDNA or FUST-1, isoform b cDNA, driven by the
279 *fust-1* original promoter (2181 bp upstream the ATG of FUST-1, isoform a). One more construct
280 with truncated N-terminal (FUST-1, ΔN) was also used (Figure S5A). Tail-expressing plasmid *lin-*
281 *44p::mRFP* was used as an injection marker. As expected, isoform a cDNA restored the mCherry
282 expression of the splicing reporter, while isoform b cDNA did not (Figure 5F, Figure S5B and
283 S5C), which confirms that FUST-1, isoform a promotes the skipping of exon-5 to produce FUST-
284 1 isoform b. Consistent with this, *fust-1* pre-mRNA, detected by primers in intron 4 of *fust-1*, was
285 significantly enriched after Co-IP with FLAG::FUST-1, which only tagged FUST-1, isoform a
286 (Figure 5G). To my surprise, the FUST-1, ΔN construct also rescued the mCherry expression, just
287 as efficient as FUST-1, isoform a (Figure 5F and Figure S5D). Since the three isoforms have

288 identical functional domains (RRM, ZnF, and NLS) with different N-terminal sequences, these
289 results suggest that the N-terminal in FUST-1, isoform b may prevent its domains from functioning
290 normally. Taken together, I characterized an autoregulation loop in *fust-1*, in which FUST-1,
291 isoform a promote the skipping of exon 5 of *fust-1* pre-mRNA, resulting in the production of
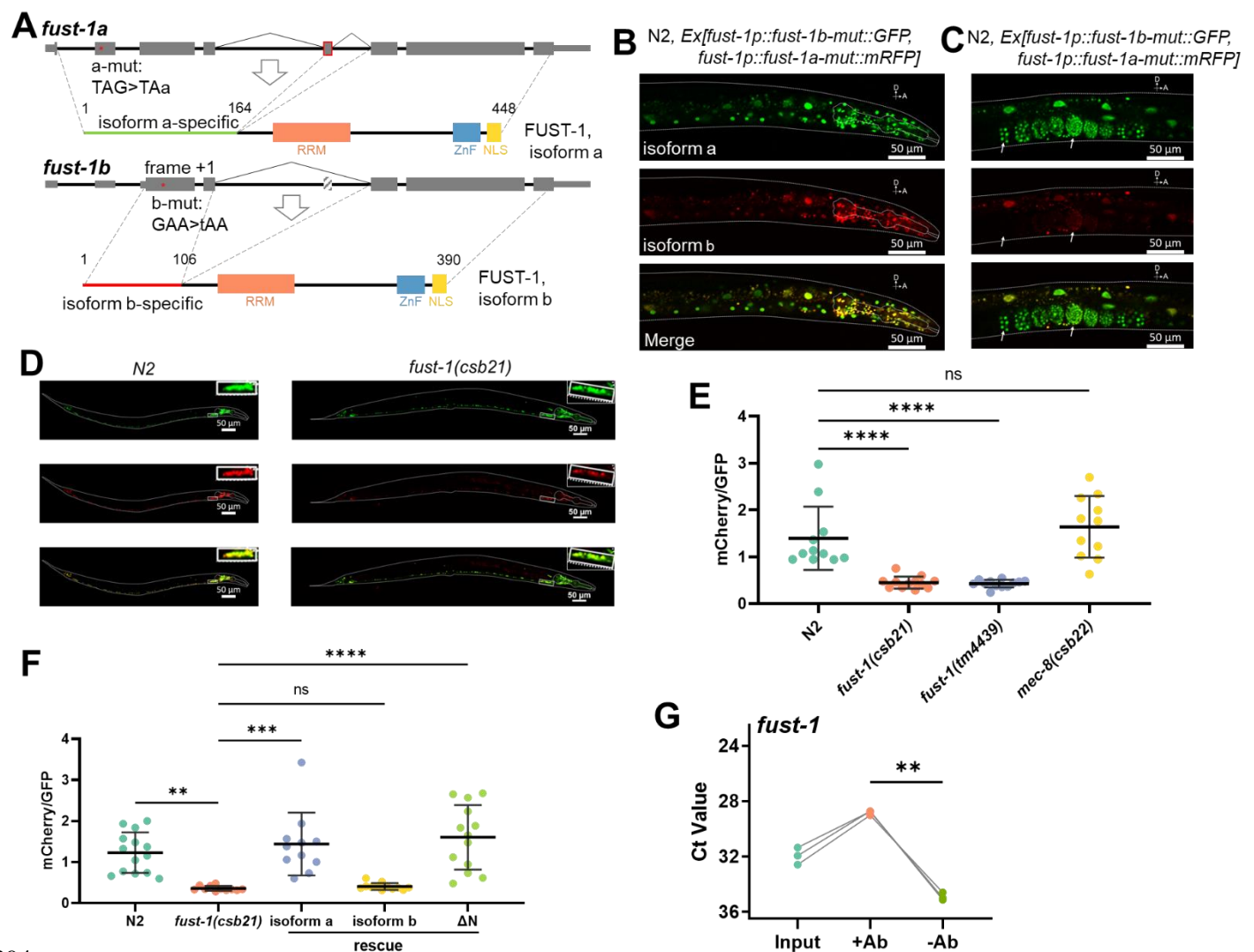292 FUST-1, isoform b.

293

294

Figure 5. An autoregulation loop in *fust-1*.

(A) Gene structure of *fust-1* and the domains in FUST-1 isoform a and isoform b. Note the positions where nonsense mutations were introduced. Lengths of amino acids in each isoform were labeled. RRM: RNA recognition motif; ZnF: Zinc-figure; NLS: nuclear localization signal.

(B, C) Confocal images showing expression of FUST-1 isoform a and isoform b in the nucleus of neuron cells (B) and eggs (C). Note that in early eggs, FUST-1 isoform a was expressed earlier than isoform b (white arrows). A: Anterior, D: Dorsal. Scale bars: 50 μm.

(D) Representative confocal images showing the expression patterns of splicing reporter of *fust-1* exon 5 in N2 strain and *fust-1(csb21)* strain. Inset squares show the enlarged neck neurons in indicated strains. A: Anterior, D: Dorsal. Scale bars: 50 μm.

305   (E, F) Quantification of mCherry-to-GFP ratios of the *fust-1* exon5 splicing reporter in the
306   indicated strains. One-way ANOVA, Tukey's multiple comparisons. $**p < 0.01$, $***p < 0.001$,
307    $****p < 0.0001$; ns, not significant.

308   (G) Ct value changes of *fust-1* pre-mRNA before and after Co-IP of FLAG::FUST-1 with or
309   without anti-FLAG antibody. Primer positions are in intron 4 of *fust-1* pre-mRNA. Results from 3
310   biological replicates are shown. Paired two-tailed Student's *t*-test. $**p < 0.01$.

311 **6. FUST-1, isoform a is the functional isoform in circRNA regulation**

312 Next, to check which isoform of FUST-1 is functional in circRNA regulation, I tried to rescue the
313 downregulated circRNAs in *fust-1(csb21)* with extrachromosomal expression of FUST-1 isoform
314 cDNA with C-terminal mRFP fusion, in which either FUST-1, isoform a, or FUST-1, isoform b
315 or FUST-1, ΔN is expressed (Figure S6A). The mRFP-positive L1 worms were sorted, from which
316 total RNA was extracted, and then circRNA levels were quantified by RT-qPCR. Same with their
317 roles in exon-skipping, FUST-1, isoform a successfully rescued the downregulated circRNAs,
318 whereas FUST-1, isoform b did not improve the downregulated circRNA levels at all, indicating
319 that FUST-1, isoform a is the functional protein in circRNA regulation (Figure 6A). Although not
320 as efficient as FUST-1, isoform a, FUST-1, ΔN fully rescued the downregulated *circ-zip-2* and
321 *circ-iglr-3* and partially restored *circ-arl-13* level (Figure 6A).

322 In an effort to generate strains with C-terminal mRFP tagging of FUST-1 isoforms, I achieved C-
323 terminal mRFP insertion in *fust-1* (*fust-1::mRFP*). Another obtained strain, in which intron 3 to
324 intron 6 of *fust-1* were removed, cannot use the autoregulation pathway, resulting in the expression
325 of only FUST-1, isoform a (*fust-1a::mRFP*) (Figure S6B). I failed to obtain a strain that can only
326 express mRFP tagged FUST-1, isoform b. Consistent with the extrachromosomal expression
327 pattern of FUST-1 (Figure 1C and Figure S1D), mRFP-tagged FUST-1 was mainly expressed in
328 the nucleus of neurons and intestinal cells (Figure S6C). Moreover, FUST-1 was also found in the
329 nucleus of gonads (Figure S6D), which was not observed in extrachromosomal expression,
330 probably due to silencing of the multicopy transgenes in the germline (Merritt and Seydoux, 2010).

331 Levels of circRNAs were compared between the two strains. Out of the five checked circRNA, the
332 levels of four circRNAs were altered in the strain only FUST-1, isoform a can be expressed (Figure
333 6B), suggesting the autoregulation loop is critical for FUST-1's role in circRNA regulation.
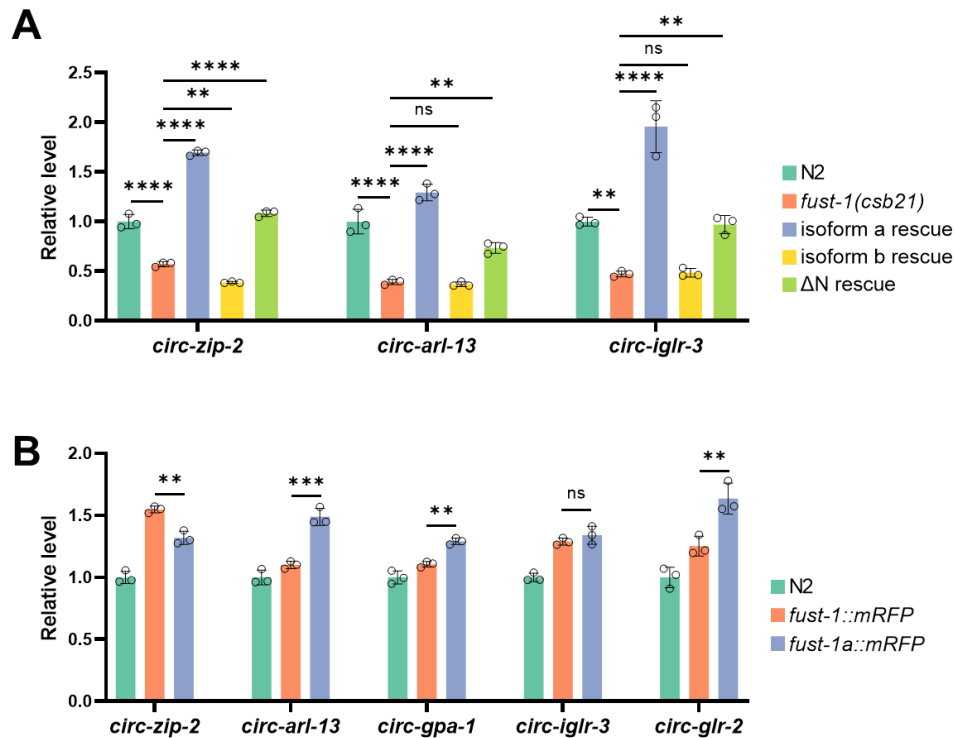
334

Figure 6. FUST-1, isoform a is the functional isoform in circRNA regulation

(A) Rescue of circRNA levels by FUST-1 isoforms, quantified by RT-qPCR. cDNA samples from L1 worms of indicated strains were used.

(B) RT-qPCR quantification of circRNA levels at the L1 stage of indicated strains. (A, B) Levels are normalized to N2 strain using *pmp-3* as the reference gene. Results are shown as mean ± sd of three biological replicates. One-way ANOVA, Tukey's multiple comparisons. **$p < 0.01$, ***$p < 0.001$, ****$p < 0.0001$; ns, not significant.

Discussion

Using identified circRNAs in the neurons as targets, I performed a small-scale screening of thirteen conserved RBP genes in their roles of circRNA regulation. Most of these RBPs showed promotional roles in circRNA production, suggesting that the involvement of RBPs in back-splicing may be common in *C. elegans*. I further showed that FUST-1, the homolog gene of FUS in *C. elegans*, regulates circRNA formation without affecting the cognate linear mRNAs (Figure 2). Although I used circRNAs either enriched in neurons or highly expressed in neurons as targets to identify FUST-1, FUST-1 did not show preference in the regulation of neuronal circRNAs (Figure 2G). Since FUST-1 is also expressed in intestine and germline cells, FUST-1 may regulate circRNAs in those cells.

CLIP-seq data on FUS suggest that rather than recognizing specific sequences, FUS tends to bind to stem-loop secondary structures (Hoell et al., 2011; Ishigaki et al., 2012; Rogelj et al., 2012; Zhou et al., 2013). In cultured N2a cells, FUS binds to the flanking introns of circularized exons (Errichelli et al., 2017). In this study, I found that FUST-1 binds to the pre-mRNAs of circRNA genes. Interestingly, I found that FUST-1 regulates both back-splicing and exon-skipping in *zip-2* and *arl-13*. In my previous work, I discovered that RCMs in circRNA-flanking introns of *zip-2* simultaneously promote both exon-skipping and back-splicing (Cao, 2021). It is possible that once FUST-1 recognizes sequences in circRNA-flanking introns in *zip-2*, it can regulate both processes at the same time.

Self-regulation has been reported in FUS, where FUS promotes skipping of exon 7 of its pre-mRNA, which results in NMD (Zhou et al., 2013). Unlike the previous example, FUST-1, isoform a-promoted exon skipping of *fust-1* pre-mRNA produces FUST-1, isoform b that contains exactly the same functional domains, but with different N-terminal sequences. While FUST-1, isoform a is capable of promoting exon-skipping and circRNA regulation, FUST-1, isoform b is not functional in either of the two aspects (Figure 5F and Figure 6A). I first hypothesized that N-terminal sequences in FUST-1, isoform a may be important for its function. However, the FUST-1, ΔN construct, which has no N-terminal sequences, seemed functional in both exon-skipping promotion and circRNA regulation, although not as efficient as FUST-1, isoform a. These results suggest that N-terminal in isoform b may interfere with the functional domain(s), possibly RRM, so that FUST-1, isoform b cannot bind to the target mRNAs recognized by FUST-1, isoform a.

The frameshifting in FUST-1, isoform b dramatically changes the N-terminal amino acid contents compared with FUST-1, isoform a. The isoform a-specific N-terminal has high ratios of glycines (53/164, 32.3%) and glutamines (22/164, 13.4%). However, isoform b-specific N-terminal contains more valines (18/106, 17.0%) and glutamic acid residues (18/106, 17.0%), which are very few in isoform a-specific N-terminal: 0/164 and 2/164, respectively. High valine content may make the N-terminal of FUST-1, isoform b more hydrophobic and high glutamic acid content can add more negative charges, which may cause the folding of FUST-1, isoform b different from isoform a. Further *in vitro* RNA binding experiments or structural analysis may be worth trying to investigate the detailed mechanisms that dictate different function potentials in the two FUST-1 isoforms.

Acknowledgment

Author Contributions

D.C. designed and conducted all the experiments, performed all the analysis, and wrote the paper.

Declaration of Interests

The author declares no competing interests.

Materials and methods

Worm maintenance

C. elegans Bristol N2 strain was used as the wild type. Worms were maintained using standard conditions on Nematode Growth Media (NGM) agar plates with *Escherichia coli* strain OP50 (Brenner, 1974) at 20°C or 25°C. New transgenic worms were generated by microinjection with ~40 ng/µl plasmid. The strains used in this study are listed in TableS1.

Plasmid preparation

fust-1p::fust-1::mRFP: fust-1 genomic fragment containing sequences from 2181bp upstream ATG to just before stop codon was cloned into the Sma I site of pHK-mRFP vector in frame with mRFP by In-Fusion HD Cloning Kit (Takara). This plasmid was further used to generate backbone structure containing *fust-1* promoter and mRFP, to which cDNAs of FUST-1 isoforms (isoform a, isoform b, and ΔN) were inserted by In-Fusion (Takara). The mRFP fused FUST-1 cDNA plasmids were used to generate cDNA only plasmids for splicing reporter rescue by removing the mRFP sequences using In-Fusion (Takara). Splicing reporter of *fust-1* exon 5 was prepared by cloning exon 4 to exon 6 into the plasmids provided by Dr. Adam Norris.

Worm synchronization

Worm synchronization was performed by bleaching for large-scale worm preparation (RNA extraction). For small-scale worm preparation (locomotion assay), worms were synchronized by egg-laying. Briefly, 10 - 15 gravid adult worms were placed onto a seeded NGM plate for four hours and worms were removed after egg-laying. The eggs were then cultured to the desired stage.

Worm sorting

L1 worms with extrachromosomal fluorescent proteins were obtained by bleaching and hatching overnight at room temperature. Then fluorescence-positive worms were sorted using BioSorter Large Particle Flow Cytometer (Union Biometrica).

Mutagenesis by CRISPR-Cas9

Mutation by CRISPR-Cas9 was performed as described previously (Cao, 2021). To make the recombinant dsDNAfragments for insertion, plasmids containing the wild-type FUST-1::mRFP were constructed first, from which dsDNA repair fragments were amplified using primers containing recombinant sequences. Guide RNA sequences, recombinant ssDNAs, validation primers, and primers for recombinant fragment amplification are listed in Table S3.

Co-immunoprecipitation (Co-IP)

~20,000 L1 FLAG::FUST-1 worms were seeded on a nutrition enriched plate with NA22 *E. coli* (NEP-NA22). After 4-day culture at 20°C, all bacteria were consumed, and most of the progenies were at the L1 stage. Adult worms were removed by filtering through a 30 µm mesh. Three NEP-NA22 plates, which gave ~ 1 million L1 worms, were used for one replicate experiment. Worms were washed with 1×10 ml M9 buffer, 2×10 ml cold Buffer B70 (50 mM HEPES-KOH (pH

434   7.4), 70 mM potassium acetate (KAc), 1 mM sodium fluoride (NaF), 20 mM β-glycerophosphate,
435   5 mM magnesium acetate (MgOAc), 0.1% Triton X-100, 10% glycerol). Worms were then re-
436   suspended in 0.4 ml Buffer B70 supplemented with $2 \times$ cOmplete Proteinase inhibitor cocktail
437   (Roche) and dripped into liquid N_2 with 1 ml pipette tips to form small pearls. Worm pearls were
438   stored at -80°C. Worm pearls were ground into fine powder in a mortar containing liquid N_2, which
439   was suspended into 1 ml cold Buffer B70 supplemented with $2 \times$ cOmplete Proteinase inhibitor
440   cocktail (Roche) and 5 μl Murine RNase Inhibitor (NEB). Worm lysate was cleared by
441   centrifugation at $20,000 \times g$ for 20 min at 4°C. 50 μl worm lysate was taken as input samples, in
442   which 40 μl was used for RNA extraction and 10 μl for western blot. 50 μl Dynabeads Protein G
443   (Invitrogen) was coupled with or without 5 μg Anti-FLAG M2 antibody (Sigma-Aldrich), which
444   was then incubated with 400 μl lysate, rotating overnight at 4°C. The next day, the lysate-beads
445   slurry was cleared magnetically, and the supernatant was taken for western blot. Keeping tubes on
446   magnetic tray, the beads were washed 2×200 ul Buffer B70 gently. 50 μl 50 mM glycine, pH 2.8
447   was added to the washed beads to elute bound RBP complex. After mixing and incubating at RT
448   for 3 min, the supernatant was transferred to another tube containing 5 μl 1 M Tris-HCl, pH 7.5
449   for pH neutralization. For the 55 μl elution, 44 μl was used for RNA extraction, 11 μl for western
450   blot.

451   Western blot

452   Protein samples were resolved by SDS-PAGE (5% stacking gel and 12% resolving gel) and
453   transferred to PVDF membrane by the standard protocol (25 V, 30 min) of Trans-Blot Turbo
454   Transfer System (Bio-Rad). After blocking with 5% BSA-PBST (137 mM Sodium Chloride, 10
455   mM Phosphate, 2.7 mM Potassium Chloride, pH 7.4, 0.1% (v/v) Tween-20, and 5% (w/v) BSA)
456   for 1 hour at room temperature, the membrane was incubated overnight with primary antibody
457   (listed below) at 4°C. After 3×5 min washes in PBST, the membrane was incubated with HRP-
458   conjugated secondary antibody at room temperature for 1 hour. The membrane was washed 3×5
459   min in PBST and then visualized by Amersham ECL Prime Western Blot Detection Reagent (GE
460   Healthcare). Images were taken by Fluorescent Image Analyzer LAS-3000 (FujiFilm) using the
461   chemiluminescence channel. Mouse ANTI-FLAG M2 antibody (F3165, Sigma-Aldrich): 1:2000;
462   Amersham ECL Mouse IgG, HRP-linked whole Ab (from sheep):1:2000.

463   RNA extraction

464   RNA extraction was performed using Direct-zol RNA MicroPrep kit (ZYMO Research) with on-
465   column DNase I (ZYMO Research) digestion according to the manufacturer's protocol. For RNA
466   extraction from worms, worms were first flash-frozen in Trizol solution (Invitrogen) in liquid N_2
467   and then homogenized by vortexing with glass beads (φ 0.1 mm) in Beads Cell Disrupter MS-100
468   (TOMY).

469   RNA Sequencing

470   For RNA-seq of samples from the L1 stage of N2 and *fust-1(csb21)*, 500 ng total RNA samples
471   from 3 biological duplicates were used as inputs. rRNA depletion was performed using Ribo-Zero
472   Plus rRNA Depletion kit (Illumina) and library preparation was conducted using NEBNext Ultra

473 II Directional RNA Library Prep Kit for Illumina (New England BioLabs) according to
474 manufacturer's protocols. Sequencing was performed on NovaSeq 6000 (Illumina) to obtain 150
475 nt paired-end reads.

476 Real-time PCR

477 Real-time PCR reactions were performed using soAdvanced Universal SYBR Green Supermix
478 (Bio-Rad) with cDNAs synthesized from iScript Advanced cDNA synthesis kit (Bio-Rad). 20 µl
479 reaction mix with 2 µl cDNA (~1-10 ng) were monitored on StepOnePlus Thermal Cycler (Applied
480 Biosystems) in "fast mode". Cycling conditions: 95 °C, 30', 40 or 45 cycles of 95 °C, 15' and 60
481 °C, 30'with plate reading, and a final melt curve stage using default conditions. If not mentioned,
482 all cDNAs used for RT-qPCR were from the L1 stage of indicated strains. If Ct values were not
483 determined or higher than Ct values in no-template control (NTC) samples, they are treated as
484 "n.d." (not detected). Primers used for RT-qPCR are listed in Table S2.

485 Northern blot

486 Northern blot was performed using NorthernMax kit (ThermoFisher Scientific) as described
487 previously (Cao, 2021). Primers used for probe amplification are in Table S2.

488 circRNA prediction and RNA-seq data analysis

489 circRNA analysis and differential expression analysis were performed as described previously
490 (Cao, 2021). In the dataset in this study, many circRNAs were predicted from *rrn-3.1*, which were
491 removed for downstream analysis. The plots (PCA plots, boxplots, scatter plots) were generated
492 using ggplot2 package (https://ggplot2.tidyverse.org/), and ggpubr
493 (http://www.sthda.com/english/rpkgs/ggpubr) package in R.

494 Microscopy

495 Confocal images were obtained using a Zeiss LSM780 confocal microscope. For mCherry-to-GFP
496 ratio quantification of splicing reporter of *fust-1* exon 5, all images were taken under the same
497 setting parameters (Pinhole: 1.00 AU; Laser: 561 nm, 2.00%, 488 nm, 2.00%; Detection
498 wavelength: GFP, 493-556 nm, mCherry, 588-694 nm; Gain: GFP, 625.0, mCherry, 790.0;
499 Detector Digital Gain: 1.0 for all channels) to make sure that no saturation in both GFP and
500 mCherry channels. Images were processed using ZEISS ZEN3.1 software. The average intensities
501 in the GFP channel and the mCherry channel were used for quantification.

502 Locomotion Assay

503 Locomotion analysis of day 3 adult worms was performed as described previously (Kawamura
504 and Maruyama, 2019). Briefly, 15 synchronized day 3 adult worms were picked onto a blank NGM
505 plate to get rid of food for ~1 min. The worms were then transferred to another empty NGM plate
506 and locomotion images were recorded for 1min with five frames with the lid on. Images were
507 analyzed using ImageJ and wrMTrck plugin (Nussbaum-Krammer et al., 2015)
508 (http://www.phage.dk/plugins/wrmtrck.html) to calculate the average speeds. More than 50 worms
509 were recorded. Worms that got lost during recording were not included.

510   Data availability

511   Raw FASTQ files from the RNA-seq data were deposited at the NCBI Sequence Read Archive
512   (BioProject: PRJNA669975, Table S4). All strains, plasmids, and other materials are available
513   upon request.

514

515

516 **References:**

517 Aktas, T., Avsar Ilik, I., Maticzka, D., Bhardwaj, V., Pessoa Rodrigues, C., Mittler, G., Manke,
518 T., Backofen, R., and Akhtar, A. (2017). DHX9 suppresses RNA processing defects originating
519 from the Alu invasion of the human genome. Nature *544*, 115-119.
520 Ashwal-Fluss, R., Meyer, M., Pamudurti, N.R., Ivanov, A., Bartok, O., Hanan, M., Evantal, N.,
521 Memczak, S., Rajewsky, N., and Kadener, S. (2014). circRNA biogenesis competes with pre-
522 mRNA splicing. Mol Cell *56*, 55-66.
523 Brenner, S. (1974). The genetics of Caenorhabditis elegans. Genetics *77*, 71-94.
524 Buratti, E., and Baralle, F.E. (2011). TDP-43: new aspects of autoregulation mechanisms in
525 RNA binding proteins and their connection with human disease. Febs J *278*, 3530-3538.
526 Cao, D. (2021). Reverse complementary matches simultaneously promote both back-splicing and
527 exon-skipping. bioRxiv, 2021.2002.2028.433292.
528 Chen, L.L. (2020). The expanding regulatory mechanisms and cellular functions of circular
529 RNAs. Nat Rev Mol Cell Biol.
530 Chen, W., and Schuman, E. (2016). Circular RNAs in Brain and Other Tissues: A Functional
531 Enigma. Trends Neurosci *39*, 597-604.
532 Cheng, J., Metge, F., and Dieterich, C. (2016). Specific identification and quantification of
533 circular RNAs from sequencing data. Bioinformatics *32*, 1094-1096.
534 Cocquerelle, C., Mascrez, B., Hetuin, D., and Bailleul, B. (1993). Mis-splicing yields circular
535 RNA molecules. Faseb J *7*, 155-160.
536 Conn, S.J., Pillman, K.A., Toubia, J., Conn, V.M., Salmanidis, M., Phillips, C.A., Roslan, S.,
537 Schreiber, A.W., Gregory, P.A., and Goodall, G.J. (2015). The RNA binding protein quaking
538 regulates formation of circRNAs. Cell *160*, 1125-1134.
539 Conn, V.M., Hugouvieux, V., Nayak, A., Conos, S.A., Capovilla, G., Cildir, G., Jourdain, A.,
540 Tergaonkar, V., Schmid, M., Zubieta, C.*, et al.* (2017). A circRNA from SEPALLATA3
541 regulates splicing of its cognate mRNA through R-loop formation. Nat Plants *3*, 17053.
542 Damianov, A., and Black, D.L. (2010). Autoregulation of Fox protein expression to produce
543 dominant negative splicing factors. Rna *16*, 405-416.
544 Dichmann, D.S., and Harland, R.M. (2012). fus/TLS orchestrates splicing of developmental
545 regulators during gastrulation. Genes Dev *26*, 1351-1363.
546 Du, W.W., Yang, W., Wu, N., Li, X., Li, F., Chen, Y., He, Q., Liu, E., Yang, Z., Fang, L.*, et al.*
547 (2020). The Circular RNA circSKA3 Binds Integrin β1 to Induce Invadopodium Formation
548 Enhancing Breast Cancer Invasion. Mol Ther.
549 Errichelli, L., Dini Modigliani, S., Laneve, P., Colantoni, A., Legnini, I., Capauto, D., Rosa, A.,
550 De Santis, R., Scarfo, R., Peruzzi, G.*, et al.* (2017). FUS affects circular RNA expression in
551 murine embryonic stem cell-derived motor neurons. Nat Commun *8*, 14741.
552 Fei, T., Chen, Y., Xiao, T., Li, W., Cato, L., Zhang, P., Cotter, M.B., Bowden, M., Lis, R.T.,
553 Zhao, S.G.*, et al.* (2017). Genome-wide CRISPR screen identifies HNRNPL as a prostate cancer
554 dependency regulating RNA splicing. Proc Natl Acad Sci U S A *114*, E5207-E5215.
555 Gruner, H., Cortes-Lopez, M., Cooper, D.A., Bauer, M., and Miura, P. (2016). CircRNA
556 accumulation in the aging mouse brain. Sci Rep *6*, 38907.
557 Hansen, T.B., Jensen, T.I., Clausen, B.H., Bramsen, J.B., Finsen, B., Damgaard, C.K., and
558 Kjems, J. (2013). Natural RNA circles function as efficient microRNA sponges. Nature *495*,
559 384-388.

560   Hoell, J.I., Larsson, E., Runge, S., Nusbaum, J.D., Duggimpudi, S., Farazi, T.A., Hafner, M.,
561   Borkhardt, A., Sander, C., and Tuschl, T. (2011). RNA targets of wild-type and mutant FET
562   family proteins. Nat Struct Mol Biol *18*, 1428-1431.
563   Ishigaki, S., Masuda, A., Fujioka, Y., Iguchi, Y., Katsuno, M., Shibata, A., Urano, F., Sobue, G.,
564   and Ohno, K. (2012). Position-dependent FUS-RNA interactions regulate alternative splicing
565   events and transcriptions. Sci Rep *2*, 529.
566   Ivanov, A., Memczak, S., Wyler, E., Torti, F., Porath, H.T., Orejuela, M.R., Piechotta, M.,
567   Levanon, E.Y., Landthaler, M., Dieterich, C.*, et al.* (2015). Analysis of intron sequences reveals
568   hallmarks of circular RNA biogenesis in animals. Cell Rep *10*, 170-177.
569   Kawamura, K., and Maruyama, I.N. (2019). Forward Genetic Screen for Caenorhabditis elegans
570   Mutants with a Shortened Locomotor Healthspan. G3-Genes Genom Genet *9*, 2415-2423.
571   Khan, M.A., Reckman, Y.J., Aufiero, S., van den Hoogenhof, M.M., van der Made, I., Beqqali,
572   A., Koolbergen, D.R., Rasmussen, T.B., van der Velden, J., Creemers, E.E.*, et al.* (2016).
573   RBM20 Regulates Circular RNA Production From the Titin Gene. Circ Res *119*, 996-1003.
574   Kramer, M.C., Liang, D., Tatomer, D.C., Gold, B., March, Z.M., Cherry, S., and Wilusz, J.E.
575   (2015). Combinatorial control of Drosophila circular RNA expression by intronic repeats,
576   hnRNPs, and SR proteins. Genes Dev *29*, 2168-2182.
577   Kwiatkowski, T.J., Bosco, D.A., LeClerc, A.L., Tamrazian, E., Vanderburg, C.R., Russ, C.,
578   Davis, A., Gilchrist, J., Kasarskis, E.J., Munsat, T.*, et al.* (2009). Mutations in the FUS/TLS
579   Gene on Chromosome 16 Cause Familial Amyotrophic Lateral Sclerosis. Science *323*, 1205-
580   1208.
581   Li, X., Liu, C.X., Xue, W., Zhang, Y., Jiang, S., Yin, Q.F., Wei, J., Yao, R.W., Yang, L., and
582   Chen, L.L. (2017). Coordinated circRNA Biogenesis and Function with NF90/NF110 in Viral
583   Infection. Mol Cell *67*, 214-227 e217.
584   Li, Z., Huang, C., Bao, C., Chen, L., Lin, M., Wang, X., Zhong, G., Yu, B., Hu, W., Dai, L.*, et
585   al.* (2015). Exon-intron circular RNAs regulate transcription in the nucleus. Nat Struct Mol Biol
586   *22*, 256-264.
587   Love, M.I., Huber, W., and Anders, S. (2014). Moderated estimation of fold change and
588   dispersion for RNA-seq data with DESeq2. Genome Biology *15*.
589   Markert, S.M., Skoruppa, M., Yu, B., Mulcahy, B., Zhen, M., Gao, S., Sendtner, M., and
590   Stigloher, C. (2019). An ALS-associated mutation in human FUS reduces neurotransmission
591   from C. elegans motor neurons to muscles. bioRxiv, 860536.
592   McGlincy, N.J., Tan, L.Y., Paul, N., Zavolan, M., Lilley, K.S., and Smith, C.W.J. (2010).
593   Expression proteomics of UPF1 knockdown in HeLa cells reveals autoregulation of hnRNP
594   A2/B1 mediated by alternative splicing resulting in nonsense-mediated mRNA decay. Bmc
595   Genomics *11*.
596   Memczak, S., Jens, M., Elefsinioti, A., Torti, F., Krueger, J., Rybak, A., Maier, L., Mackowiak,
597   S.D., Gregersen, L.H., Munschauer, M.*, et al.* (2013). Circular RNAs are a large class of animal
598   RNAs with regulatory potency. Nature *495*, 333-338.
599   Merritt, C., and Seydoux, G. (2010). Transgenic solutions for the germline. WormBook, 1-21.
600   Muller-McNicoll, M., Rossbach, O., Hui, J.Y., and Medenbach, J. (2019). Auto-regulatory
601   feedback by RNA-binding proteins. J Mol Cell Biol *11*, 930-939.
602   Murakami, T., Qamar, S., Lin, J.Q., Schierle, G.S.K., Rees, E., Miyashita, A., Costa, A.R., Dodd,
603   R.B., Chan, F.T.S., Michel, C.H.*, et al.* (2015). ALS/FTD Mutation-Induced Phase Transition of
604   FUS Liquid Droplets and Reversible Hydrogels into Irreversible Hydrogels Impairs RNP
605   Granule Function. Neuron *88*, 678-690.

606   Murakami, T., Yang, S.P., Xie, L., Kawano, T., Fu, D., Mukai, A., Bohm, C., Chen, F.S.,
607   Robertson, J., Suzuki, H.*, et al.* (2012). ALS mutations in FUS cause neuronal dysfunction and
608   death in Caenorhabditis elegans by a dominant gain-of-function mechanism. Hum Mol Genet *21*,
609   1-9.
610   Nigro, J.M., Cho, K.R., Fearon, E.R., Kern, S.E., Ruppert, J.M., Oliner, J.D., Kinzler, K.W., and
611   Vogelstein, B. (1991). Scrambled exons. Cell *64*, 607-613.
612   Norris, A.D., Gao, S., Norris, M.L., Ray, D., Ramani, A.K., Fraser, A.G., Morris, Q., Hughes,
613   T.R., Zhen, M., and Calarco, J.A. (2014). A Pair of RNA-Binding Proteins Controls Networks of
614   Splicing Events Contributing to Specialization of Neural Cell Types. Mol Cell *54*, 946-959.
615   Norris, A.D., Gracida, X., and Calarco, J.A. (2017). CRISPR-mediated genetic interaction
616   profiling identifies RNA binding proteins controlling metazoan fitness. Elife *6*, e28129.
617   Nussbaum-Krammer, C.I., Neto, M.F., Brielmann, R.M., Pedersen, J.S., and Morimoto, R.I.
618   (2015). Investigating the Spreading and Toxicity of Prion-like Proteins Using the Metazoan
619   Model Organism C. elegans. Jove-J Vis Exp.
620   Okholm, T.L.H., Sathe, S., Park, S.S., Kamstrup, A.B., Rasmussen, A.M., Shankar, A., Chua,
621   Z.M., Fristrup, N., Nielsen, M.M., Vang, S.*, et al.* (2020). Transcriptome-wide profiles of
622   circular RNA and RNA-binding protein interactions reveal effects on circular RNA biogenesis
623   and cancer pathway expression. Genome Med *12*.
624   Rogelj, B., Easton, L.E., Bogu, G.K., Stanton, L.W., Rot, G., Curk, T., Zupan, B., Sugimoto, Y.,
625   Modic, M., Haberman, N.*, et al.* (2012). Widespread binding of FUS along nascent RNA
626   regulates alternative splicing in the brain. Sci Rep *2*, 603.
627   Rossbach, O., Hung, L.H., Schreiner, S., Grishina, I., Heiner, M., Hui, J.Y., and Bindereif, A.
628   (2009). Auto- and Cross-Regulation of the hnRNP L Proteins by Alternative Splicing. Mol Cell
629   Biol *29*, 1442-1451.
630   Rybak-Wolf, A., Stottmeister, C., Glazar, P., Jens, M., Pino, N., Giusti, S., Hanan, M., Behm,
631   M., Bartok, O., Ashwal-Fluss, R.*, et al.* (2015). Circular RNAs in the Mammalian Brain Are
632   Highly Abundant, Conserved, and Dynamically Expressed. Mol Cell *58*, 870-885.
633   Sama, R.R.K., Ward, C.L., and Bosco, D.A. (2014). Functions of FUS/TLS From DNA Repair
634   to Stress Response: Implications for ALS. Asn Neuro *6*.
635   Sureau, A., Gattoni, R., Dooghe, Y., Stevenin, J., and Soret, J. (2001). SC35 autoregulates its
636   expression by promoting splicing events that destabilize its mRNAs. Embo Journal *20*, 1785-
637   1796.
638   Tan, J.H., and Fraser, A.G. (2017). The combinatorial control of alternative splicing in C.
639   elegans. Plos Genet *13*.
640   Therrien, M., Rouleau, G.A., Dion, P.A., and Parker, J.A. (2016). FET proteins regulate lifespan
641   and neuronal integrity. Sci Rep *6*, 25159.
642   Thompson, M., Bixby, R., Dalton, R., Vandenburg, A., Calarco, J.A., and Norris, A.D. (2019).
643   Splicing in a single neuron is coordinately controlled by RNA binding proteins and transcription
644   factors. Elife *8*.
645   Vaccaro, A., Patten, S.A., Ciura, S., Maios, C., Therrien, M., Drapeau, P., Kabashi, E., and
646   Parker, J.A. (2012a). Methylene Blue Protects against TDP-43 and FUS Neuronal Toxicity in C.
647   elegans and D. rerio. Plos One *7*.
648   Vaccaro, A., Tauffenberger, A., Aggad, D., Rouleau, G., Drapeau, P., and Parker, J.A. (2012b).
649   Mutant TDP-43 and FUS Cause Age-Dependent Paralysis and Neurodegeneration in C. elegans.
650   Plos One *7*.

651 Vance, C., Rogelj, B., Hortobagyi, T., De Vos, K.J., Nishimura, A.L., Sreedharan, J., Hu, X.,
652 Smith, B., Ruddy, D., Wright, P.*, et al.* (2009). Mutations in FUS, an RNA Processing Protein,
653 Cause Familial Amyotrophic Lateral Sclerosis Type 6. Science *323*, 1208-1211.
654 Veriepe, J., Fossouo, L., and Parker, J.A. (2015). Neurodegeneration in C-elegans models of
655 ALS requires TIR-1/Sarm1 immune pathway activation in neurons. Nat Commun *6*.
656 Westholm, J.O., Miura, P., Olson, S., Shenker, S., Joseph, B., Sanfilippo, P., Celniker, S.E.,
657 Graveley, B.R., and Lai, E.C. (2014). Genome-wide analysis of drosophila circular RNAs
658 reveals their structural and sequence properties and age-dependent neural accumulation. Cell Rep
659 *9*, 1966-1980.
660 Wollerton, M.C., Gooding, C., Wagner, E.J., Garcia-Blanco, M.A., and Smith, C.W.J. (2004).
661 Autoregulation of polypyrimidine tract binding protein by alternative splicing leading to
662 nonsense-mediated decay. Mol Cell *13*, 91-100.
663 Xia, P., Wang, S., Ye, B., Du, Y., Li, C., Xiong, Z., Qu, Y., and Fan, Z. (2018). A Circular RNA
664 Protects Dormant Hematopoietic Stem Cells from DNA Sensor cGAS-Mediated Exhaustion.
665 Immunity *48*, 688-701 e687.
666 You, X., Vlatkovic, I., Babic, A., Will, T., Epstein, I., Tushev, G., Akbalik, G., Wang, M.,
667 Glock, C., Quedenau, C.*, et al.* (2015). Neural circular RNAs are derived from synaptic genes
668 and regulated by development and plasticity. Nat Neurosci *18*, 603-610.
669 Zhang, T., Wu, Y.C., Mullane, P., Ji, Y.J., Liu, H., He, L., Arora, A., Hwang, H.Y., Alessi, A.F.,
670 Niaki, A.G.*, et al.* (2018). FUS Regulates Activity of MicroRNA-Mediated Gene Silencing. Mol
671 Cell *69*, 787-801 e788.
672 Zhou, Y.Q., Liu, S.Y., Liu, G.D., Ozturk, A., and Hicks, G.G. (2013). ALS-Associated FUS
673 Mutations Result in Compromised FUS Alternative Splicing and Autoregulation. Plos Genet *9*.
674 Zhu, Y.-J., Zheng, B., Luo, G.-J., Ma, X.-K., Lu, X.-Y., Lin, X.-M., Yang, S., Zhao, Q., Wu, T.,
675 Li, Z.-X.*, et al.* (2019). Circular RNAs negatively regulate cancer stem cells by physically
676 binding FMRP against CCAR1 complex in hepatocellular carcinoma. Theranostics *9*, 3526-
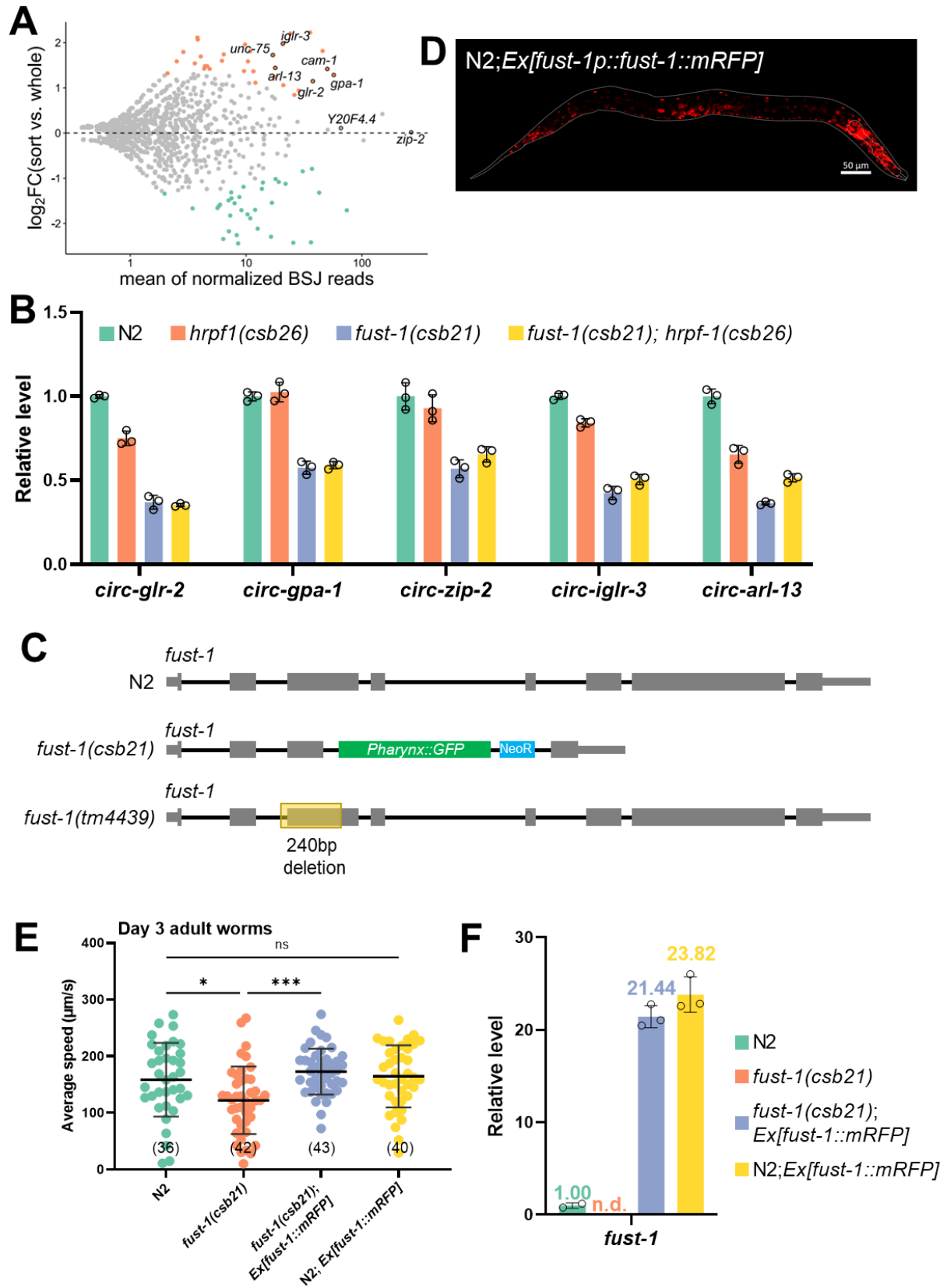677 3540.
678

Figure S1: Related to Figure 1.

(A) Differentially expressed circRNAs between sorted neuron samples and whole worm samples. Colored dots represent significantly differentially expressed circRNAs.

(B) RT-qPCR quantification of circRNA levels at L1 stage of indicated strains. Note that there is no additive effect in *fust-1(csb21); hrpf-1(csb26)* double mutant strain compared with *fust-1(csb21)* strain. Levels are normalized to the N2 strain using *pmp-3* as the reference gene. Results are shown as mean ± sd of three biological replicates.

(C) Gene structure of *fust-1* in wildtype N2 strain, *fust-1(csb21)*, and *fust-1(tm4439)* strain.

(D) Representative image showing mRFP-fused FUST-1 in wildtype N2 strain. Scale bar: 50 μm.

(E) Average moving speed of day 3 adult worms raised at 25°C with the indicated genotypes. Numbers in brackets are numbers of worms used for moving speed measurement. Results are shown as mean ± sd. One-way ANOVA, Tukey's multiple comparisons. $*p<0.05$, $***p < 0.001$, ns, not significant.

(F) RT-qPCR quantification of fust-1 mRNA levels at the L1 stage of indicated strains. Levels are normalized to the N2 strain using *pmp-3* as the reference gene. Results are shown as mean ± sd of three biological replicates. n.d.: not detected.
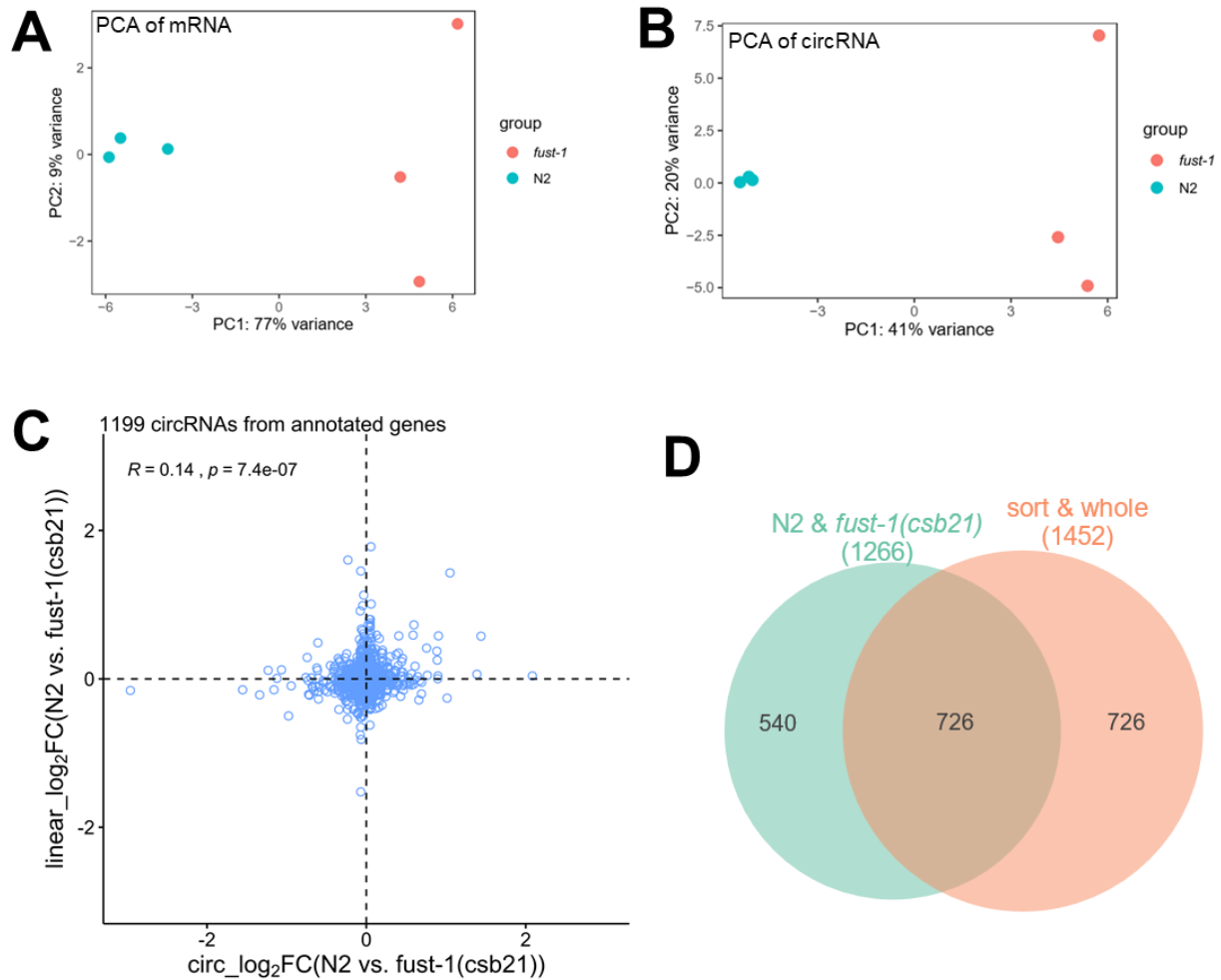
Figure S2: related to Figure 2.

(A, B) Principal component analysis of linear mRNAs (A) and circRNAs (B) between wildtype N2 strain and *fust-1(csb21)* strain.

(C) Scatter plot showing the log2 fold changes of all circRNAs versus log2 fold changes of their cognate linear mRNAs. The Pearson correlation coefficient (*R*) and *p* value (*p*) are shown.

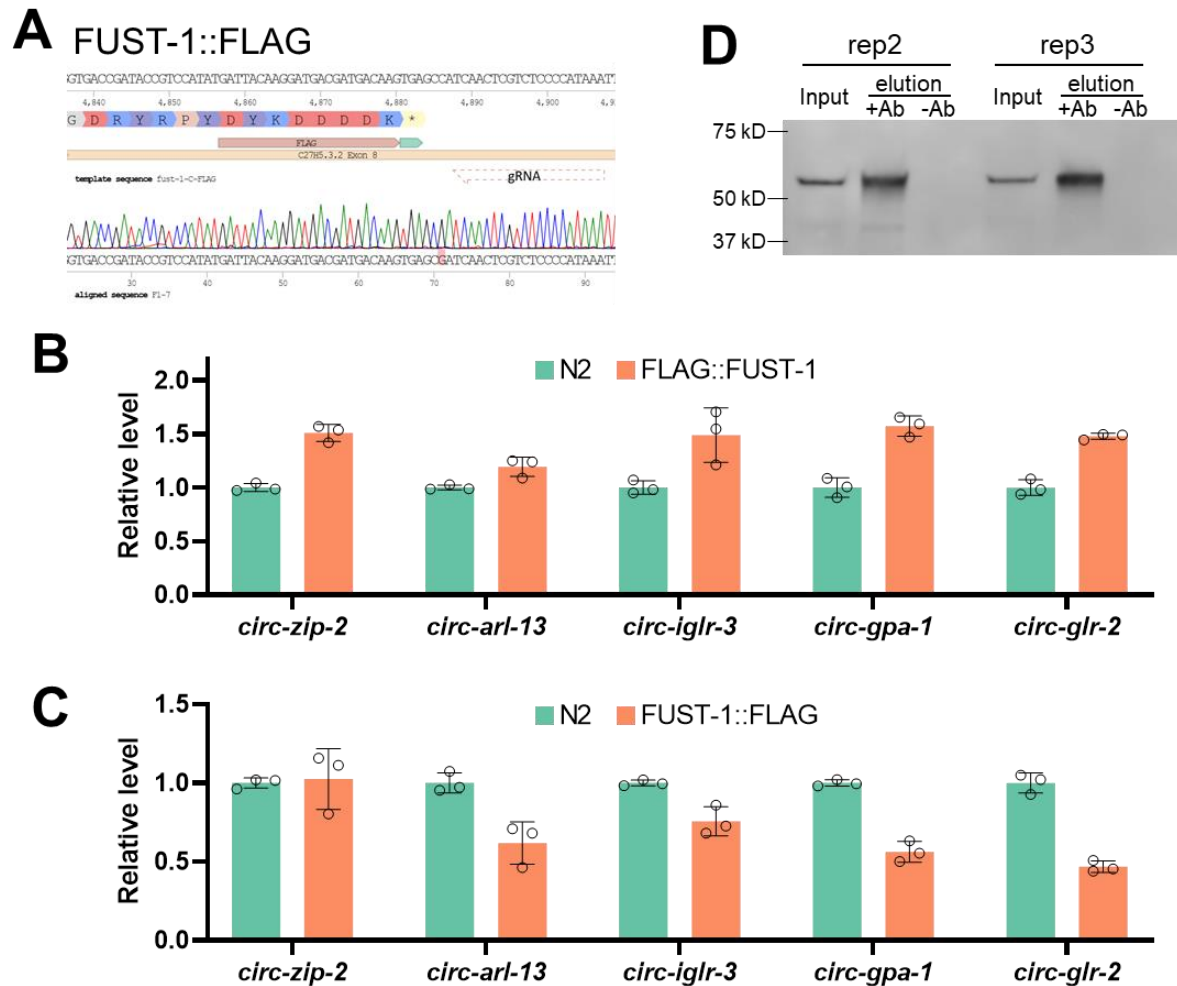(D) Venn diagram showing overlapped circRNAs between the "*N2-fust-1(csb21)*" dataset and the "sort & whole" dataset.

Figure S3: related to Figure 3.

(A) Sequence confirmation of C-terminal fusion of FLAG tag just before the stop codon of FUST-1. Note the position of gRNA and the mutated PAM site (TGG>TCG).

(B, C) RT-qPCR quantification of circRNA levels between wildtype N2 strain and N-terminal FLAG fusion of FUST-1 strain (B) and between wildtype N2 strain and C-terminal FLAG fusion of FUST-1 strain (C). Levels are normalized to the N2 strain using *pmp-3* as the reference gene. Results are shown as mean ± sd of three biological replicates.

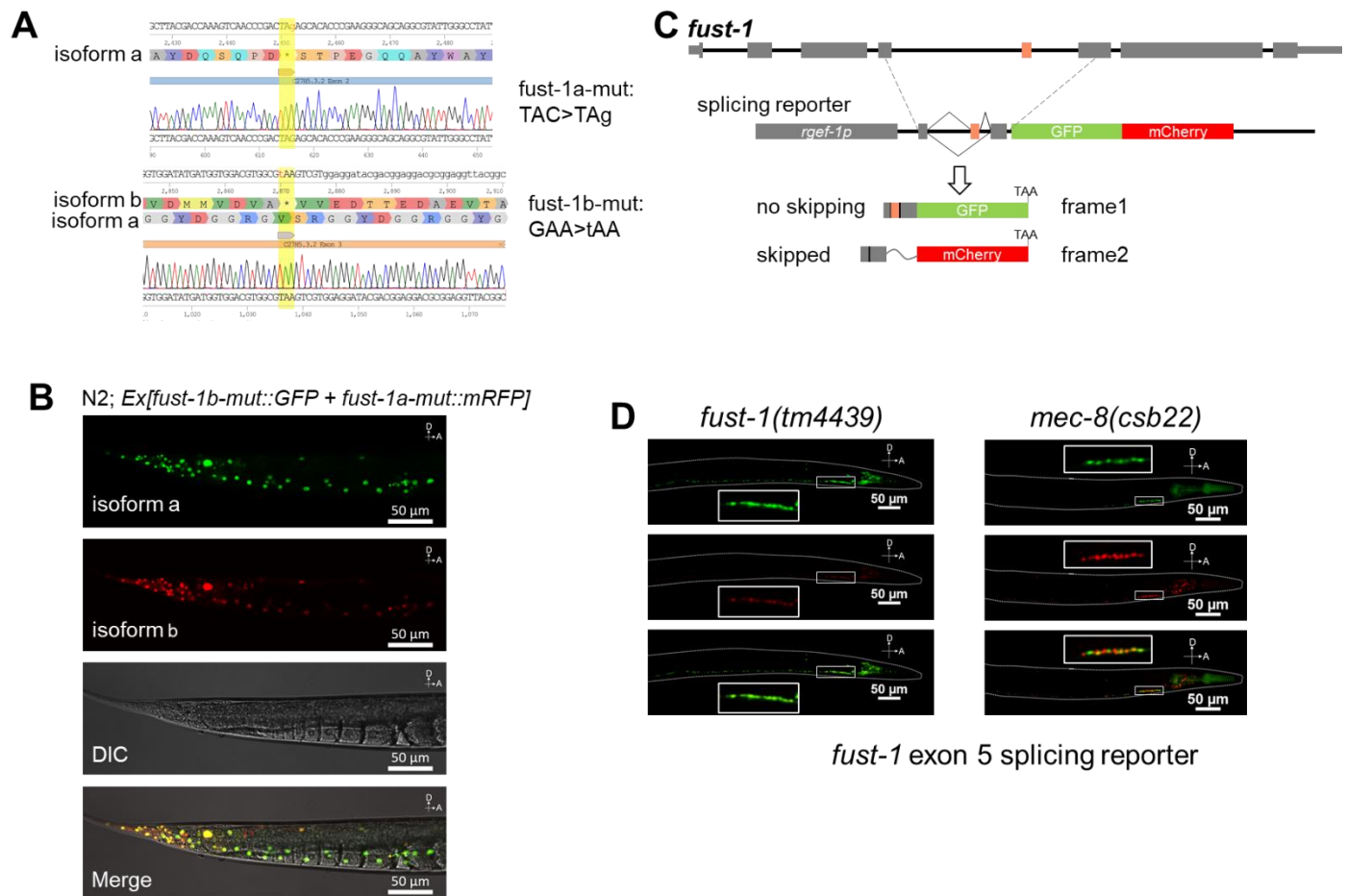(D) Western blot of the other two biological replicates of FLAG::FUST-1 Co-IP with or without FLAG antibody.

Figure S4: related to Figure 5

(A) Sequence confirmation of *fust-1a-mut::mRFP* plasmid and *fust-1b-mut::GFP* plasmid. The mutated sites are in yellow shadows. Note the introduction of the stop codons in the read frame of isoform a and isoform b.

(B) Confocal images showing expression of FUST-1 isoform a and isoform b in the tail. A: Anterior, D: Dorsal. Scale bars: 50 μm.

(C) Illustration of the dual-color splicing reporter of *fust-1* exon 5.

(D) Representative images showing the expression patterns of splicing reporter of *fust-1* exon 5 in *fust-1(csb21)* strain and *fust-1(tm4439)* strain. Inset squares show the enlarged neck neurons. A: Anterior, D: Dorsal. Scale bars: 50 μm.
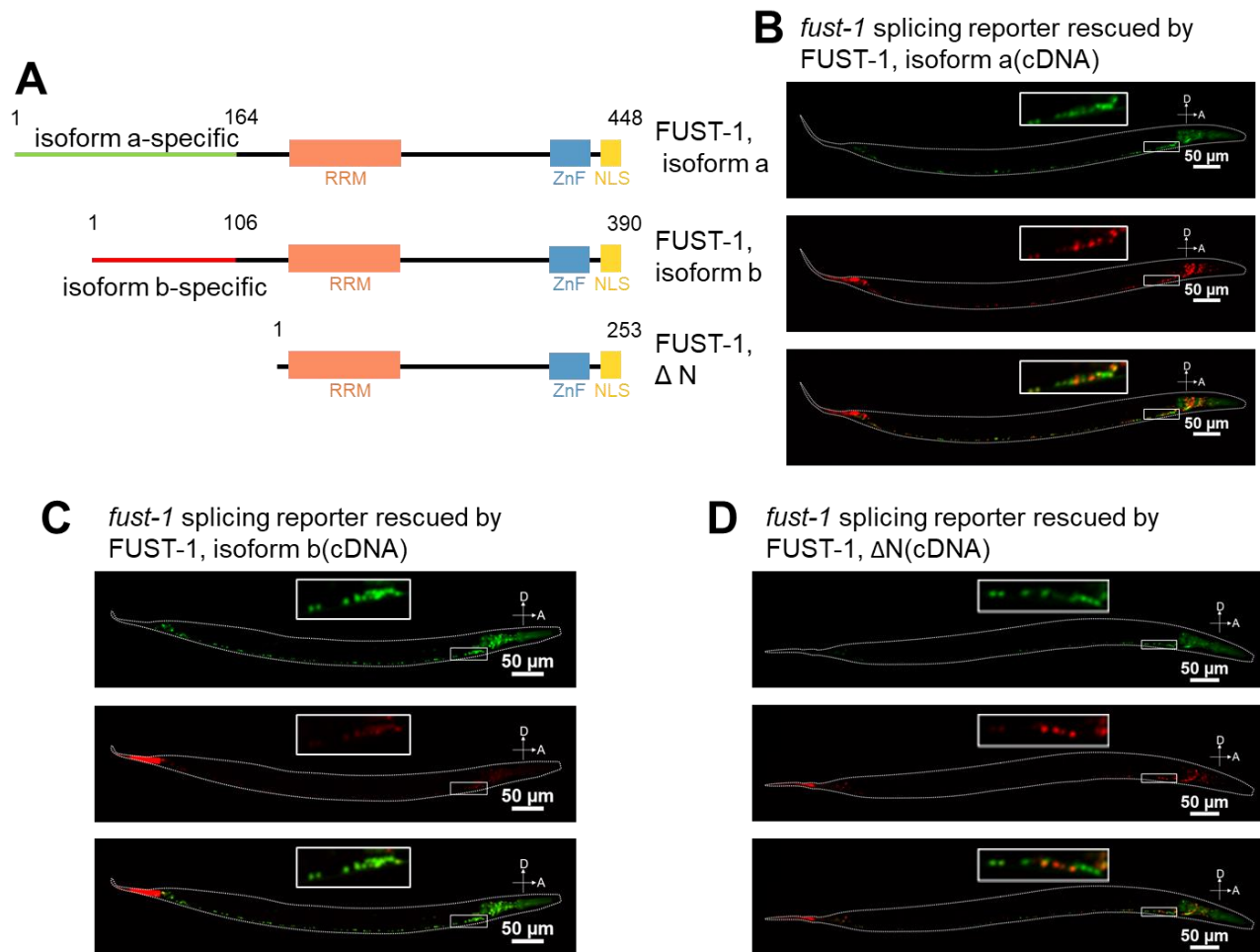
Figure S5: related to Figure 5.

(A) Domains in three FUST-1 constructs. The lengths of the constructs are labeled.

(B, C, and D) Representative confocal images showing rescue of *fust-1* exon 5 splicing reporter in FUST-1(csb21) strain by FUST-1, isoform a (B), FUST-1, isoform b (C), and by FUST-1, ΔN (D). Inset squares show the enlarged neck neurons in indicated strains. A: Anterior, D: Dorsal. Scale bars: 50 μm.
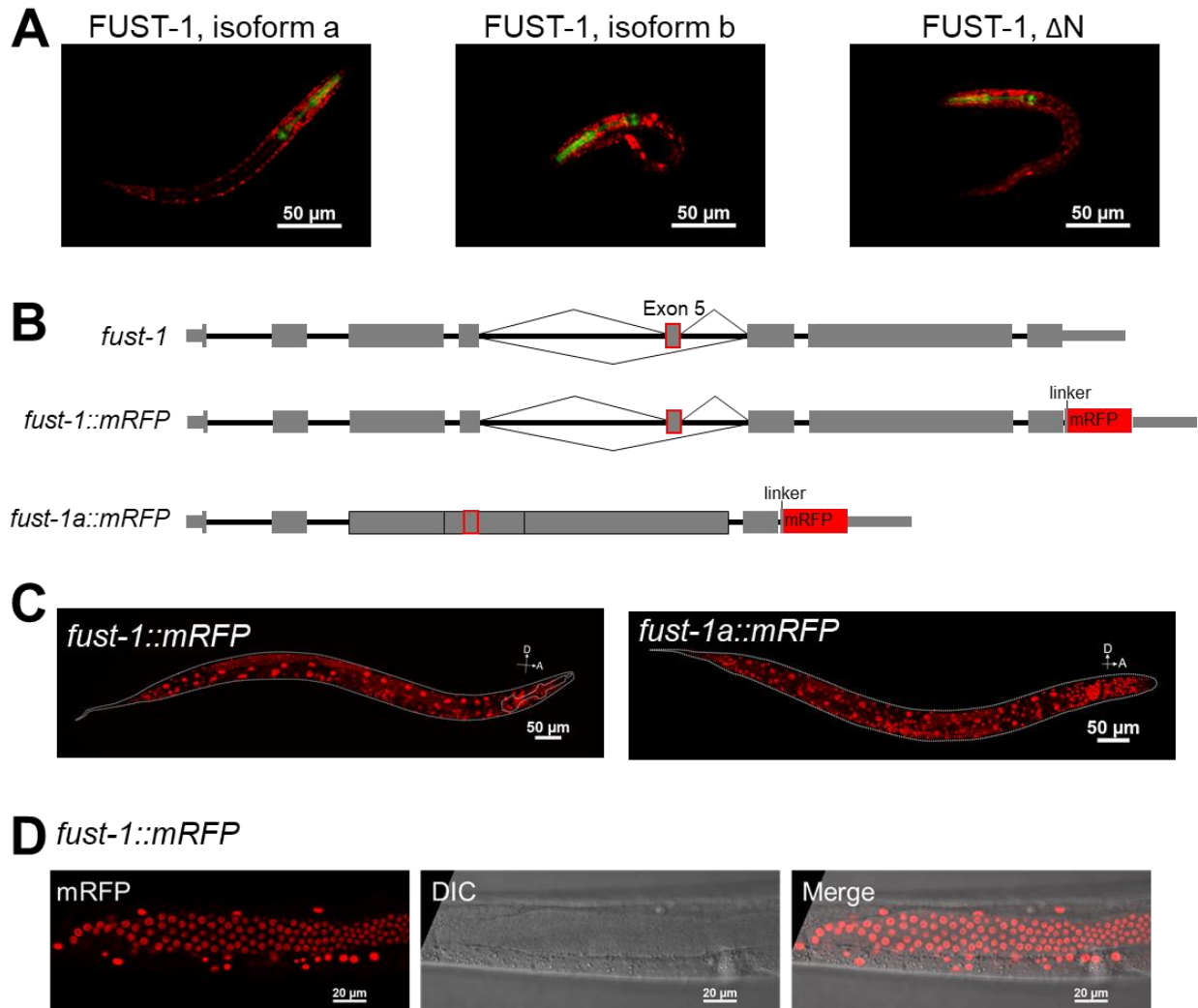
Figure S6: Related to Figure 6

(A) Representative confocal images of rescue strains with extrachromosomal expressions of mRFP fused cDNA of FUST-1 isoforms in the *fust-1(csb21)* strain. Note the expression of pharyngeal GFP. Worms were at the L1 stage. Scale bars: 50 μm.

(B) Illustration of the gene structures of *fust-1* in wildtype N2 strain, C-terminal mRFP fused *fust-1* (*fust-1::mRFP*) strain, and the strain can only express FUST1-, isoform a (*fust-1a::mRFP*).

(C) Representative images showing expression patterns of FUST-1 in the indicated strains. A: Anterior, D: Dorsal. Scale bars: 50 μm.

(D) Confocal images showing that FUST-1 is expressed in the gonad. Scale bar: 20 μm.